Design of Integrated Geothermal- Solar Based System for Multigenerational Needs in a District Energy System Application

Hamed Alimoradiyan

Submitted to the
Institute of Graduate Studies and Research
in partial fulfillment of the requirements for the degree of

Master of Science
in
Mechanical Engineering

Eastern Mediterranean University
July 2016
Gazimağusa, North Cyprus

Approval of the Institute of Graduate Studies and Research

Prof. Dr. Cem Tanova
Acting Director

I certify that this thesis satisfies the requirements as a thesis for the degree of Master of Science in Mechanical Engineering.

Assoc. Prof. Dr. Hasan Hacışevki
Chair, Department of Mechanical Engineering

We certify that we have read this thesis and that in our opinion it is fully adequate in scope and quality as a thesis for the degree of Master of Science in Mechanical Engineering.

Assoc. Prof. Dr. Hasan Hacışevki
Supervisor

Examining Committee

1. Prof. Dr. Fuat Egelioğlu

2. Assoc. Prof. Dr. Hasan Hacışevki

3. Asst. Prof. Dr. Murat Özdenefe

ABSTRACT

The current thesis proposes an integrated geothermal based multi-generation system including the triple effect LiBr/water absorption system (TEAS), organic Rankine cycle (ORC), air-conditioning system (dehumidification with cooling) and an electrolyzer. The aim of this system is to supply six outputs comprising heating, cooling, dry air, hot water, hydrogen, and power. All the simulations are done by Engineering Equation Solver software (EES). By inputting 500K geothermal water, the energetic and exergetic overall utilization factors ($\mathcal{E}_{en}$ and $\mathcal{E}_{ex}$) for the completely multi-generation cycle would be 2.467 and 1.097, respectively. A parametric study was conducted indicating that a rise in the environment (ambient) temperature from 295K to 320K leads to an accumulative trend for exergetic coefficient of performance (COP_{ex}) while energetic coefficient of performance (COP_{en}) remains constant in TEAS. While, the evaporator temperature rises from 274K to 279K, there is a downward trend for COP_{en} and COP_{ex} (from 1.491 to 1.479 and 0.3525 to 0.3145, respectively) as well as $\mathcal{E}_{en}$ and $\mathcal{E}_{ex}$. By raising the geothermal temperature from 400K to 500K, $\mathcal{E}_{en}$ and $\mathcal{E}_{ex}$ will increase from 2.354 to 2.467 and from 1.055 to 1.105, respectively. Moreover, the rise in geothermal temperature will upsurge the rate of hydrogen production as well as the heat rate in hot water production from 0.004873L/s to 0.005944L/s and from 8.365kW to 112.9kW, respectively. Moreover, environmental impacts, as one of the most designing parameter, are analyzed to find the system irreversibility (exergy destruction) and exergy losses. The parametric simulation is done to check the system in term of environmental suitability. In addition, a comparative study shows that using multi-generation cycle with higher

COP_{en} and COP_{ex} in comparison with conventional systems is more feasible to design for reaching the six outputs.

Keywords: Geothermal, Multi-generation, Energy, Exergy, Overall Utilization Factor, Exergoenvironmental Impact Factors.

ÖZ

Bu çalışma çoklu jenerasyon sistemi ile üçlü etkili LiBr/su absorbsiyon sisteminin (TEAS) birleştirilmiş organik Rankin döngüsü (ORC), klima sistemi (soğutma ile nem alma) ve elektrolizer ile jeotermal tabanlı sistemlerin birleştirilmesini öngörmektedir. Bu sistemin amacı elde edilmesidin adet sonucun: ısıtma, soğutma, kuru hava, sıcak su, hidrojen ve gücün. 500K derecede jeotermal suyun enjekte edilmesi ile genel enerjik ve ekzerjik kullanım faktörleri (Ɛen ve Ɛex) sırası ile 2.467 ve 1.097 olacaktır. Üçlü etkili LiBr/su absorbsiyon sisteminin (TEAS) yapılan parametrik çalışma çevre ısısının 295K den 320K'e çıkması ekzerjik performans katsayısının (COPex) arttığını ancak enerjik performans katsayısının (COPen) ise sabit kaldığını göstermiştir. Dolayısı ile çevre sıcaklığı arttığında Ɛen sabit kalırken değişen her jeotermal kütle akışında Ɛen artacaktır, Bunun yanında buharlaştırıcı sıcaklığı 274K den 279K'e arttığında COPen ve COPex (1.491 den 1.479'a ve 0.3525 den 0.3145'e) ayrıca Ɛen ve Ɛex sırası ile azalır. Soğutma yükü de 413.18kW'dan 410.4kW değerine düşerken klima sisteminde yoğunlaşan su miktarı artmaktadır. Jeotermal sıcaklığı 400K den 500K'e yükseltmekle Ɛen 2.354 den 2.467 ye ve Ɛex 1.055 den 1.105 ye sırası ile artacaktır. Ayrıca jeotermal sıcaklıktaki yükselme hidrojen üretim oranı 0.004873L/s den 0.005944L/s ye, sıcak su üretimindeki ısı oranını 8.365kW dan 112.9kW'a artıracaktır. Bunların yanında çevre etkisi de en önemli tasarım parametrelerinden biridir ve sistem geridönüşümsüzlüğünü (ekzerji imhası) ve ekzerji kayıplarını bulmak için analiz edilmiştir. Sistemin çevresel uygunluğu için parametrik simülasyon yapılmıştır. Ek olarak yapılan mukayese çalışması göstermiştir ki yüksek COPen ve COPex li çoklu

generasyon döngüsü konvansiyonel sisteme göre istenen altı sonuca varmada daha uygulanabilir görülmektedir.

Anahtar kelimeler: Jeotermal, Çoklu jenerasyon, Enerji, Ekzerji, Genel kullanım faktörü ve Ekzergoçevre faktörü.

ACKNOWLEDGMENT

I would like to record my gratitude to Assoc. Prof. Dr. Hasan Hacışevki for his supervision, advice, and guidance from the very early stage of this thesis as well as giving me extraordinary experiences throughout the work. Above all and the most needed, he provided me constant encouragement and support in various ways. His ideas, experiences, and passions have truly inspired and enriched my growth as a student. I am indebted to him more than he knows.

Special thanks go to Asst. Prof. Dr. Tahir Abdul Hussain Ratlamwala for his crucial contribution and guidance to this study.

Last but not the least; I would like to thank my family members specially my parents for all their supports throughout my life.

TABLE OF CONTENTS

LIST OF TABLES

LIST OF FIGURES

LIST OF ABBREVIATIONS

COP	Coefficient of Performance
$\dot{E}x_{di}$	Exergy Destruction Rate (kW)
$\dot{E}n$	Energy Rate (kW)
$\dot{E}x$	Exergy Rate (kW)
H	Specific Enthalpy, kJ/kg
HW	Hot Water
$\dot{m}$	Mass Flow Rate (kg/s)
P	Pressure (kPa)
$\dot{Q}$	Heat Flow Rate (kW)
T	Temperature (K)
S	Specific Entropy (kJ/kg K)
$\dot{W}$	Work Amount (kW)

Greek letters

H	Efficiency
ω	specific Ratio (%)
ε	Overall Utilization Factor

Subscripts

Abso	Absorber
Cond	Condenser
En	Energy
Ex	Exergy
Eva	Evaporator
Geo	Geothermal

HHX	High Temperature Heat Exchanger
HTG	High Temperature Generator
HW	Hot Water
H_2	Hydrogen
LHX	Low Temperature Heat Exchanger
LTG	Low Temperature Generator
MHX	Medium Temperature Heat Exchanger
MTG	Medium Temperature Generator
P	Pump
Ph	Physical
Turb	Turbine
W	Water
X	Concentration of Ammonia–Water
1,. . .,46	State Numbers
0	Ambient or Reference Condition

Acronyms

TEAS	Triple Effect Absorption System

Chapter 1

INTRODUCTION

1.1 Overview

Nowadays, by considering the size of mega-cities and high rate of population growth all around the world, energy consumption has become a crucial concern for nations around the world. The high pace development in the industrial era has enhanced the energy demand more than before in the last decades. To supply energy needs in the recent years, using fossil fuels including the environmental impacts such as emitting greenhouse gasses, global warming, and ozone depletion, have become increased because of their high efficiency performance and accessibility.

Global warming, as one of the important environmental threats, clarifies to an increase in the temperature average of the environment, which has been peered recently and it is raising so fast these days, Green (environmental) activities are trying to find new techniques and ways to defeat the atmospheric problem including greenhouse gases (GHGs) and aerosols. A greenhouse gas in the atmosphere can absorb the sun radiation and release it as infrared waves [1]. Global warming is directly affected by GHGs.

The global warming can be created by the following reasons [2]:

- Carbon dioxide emitted from utilities because of burning fossil fuels

- Carbon dioxide emitted from transportation systems because of burning gasoline
- Methane can be produced by animals, agricultural activities, and from sea beds
- Destroying forests especially in tropical areas to produce wood, pulp and making farmland
- Using chemical fertilizer on croplands

It has become so crucial to define new ways to supply energy demands like alternative energy sources, which are energy efficient and environmentally friend without harmful impacts on the nature and its living creatures [3].

Integrated energy system refers to a system that is capable to drive a multi-generation energy cycle to produce heating load by using two or more initial energy resources. In a cogeneration cycles, overall energy efficiency is the portion of the input energy to the exit amount of the electricity and thermal energy, is near to the 50% [4].

Lately, combined heat and power energy systems (CHPs), that are capable to produce heating and power, have been up graded and extended to the tri-generation systems by the energy researchers to produce three useful outputs including thermal energy, cooling and power generation from a basic energy. These systems use the output waste heat of utilities to improve the overall thermal efficiency [5]. The cooling and heating equipment in a tri-generation system can be run by the extra heat from system's impetus [6].

The produced heat can be used for heating process (steam production) or domestic hot water and space heating. In addition, the absorption chiller can produce cooling by the injection of the produced heat. Tri-generation systems can be utilized in several aspects such as domestic usage, hospitals, airports, hotels, food industries and chemical process. The next step in this science is Multi-generation Cycles. Multi-generation is a system with higher variety of outputs in comparison with tri-generation systems. A multi-generation system is capable to generate power process heat, cooling, hydrogen, dried air, and water desalination. In multi-generation cycles, the efficiency is significantly higher than CHPs and trig-generation systems due to its extra outputs (water desalination, hydrogen, etc.). In order to produce hydrogen, it is needed to install an electrolyzer that requires electricity. The heating load is referred to two parts of space heating and hot water production. Absorption system receives available waste heat rejected to produce cooling for the domestic purpose and cooling for the air-drying systems or chillers. To produce drinkable fresh (potable) water from multigeneration energy system, it is needed to consider desalination equipment. In this way, a part of the produced or waste heat is used to drive the desalination system, and a portion of the generated electricity is used to run the moving pumps.

1.2 Multi-generation Energy System

Multi-generation energy system refers to a system which is capable to produce more than three outputs with the same prime mover. These outputs can be electricity, heating, cooling, hydrogen, dry air and hot water. This system can be installed for residential, commercial and some other places that several useful outputs are needed. In order to design a multi-generation system, its location, type initial source and number of needed outputs should be considered. These systems are considered as a

solution of global warming and environmental concerns. The optimization methods can be considered in designing process to increase the system efficiency.

1.3 Benefit of Multi-generation Cycles

Multi-generation energy systems can be so useful and beneficial due to some parameters such as less waste and thermal losses, higher energy and exergy efficiency, less greenhouse gas emissions, less operating expenses, better resource usage, shorter delivery units, and several multiple-production choices [7].

These points are discussed in more details below. Multi-generation design increases the total energy and exergy efficiency of the utility and decreases the operation and maintenance costs. The overall energy efficiency of the conventional utilities that burn fossil fuels in a lone main impetus is generally around 40%. It shows that about half of the thermal energy injected to a primary energy system will be the waste energy and not used in any parts. The total energy efficiency of the primary utility that generates the heat and electricity in parallel can be near to the 60% [8].

It is inevitable that by using the thermal losses and waste heat from the main parts of the system, the overall energy efficiency of the power the multi-generation systems can reach up to 80% [9]. In a multi-generation energy system, the thermal energy heat produced by some renewable resources is used to run absorption system to produce heating and cooling but in a conventional utility fuel injection is needed to run the system. Therefore, a multi-generation power plant has higher overall performance compared to other power generation systems.

The efficiencies of multi-generation systems are higher compared to other power generation systems. Therefore, it can be said that multi-generation systems are friendly to the environment.

By considering some important limitation of designing multi-generation utilities in the distribution parts due to their internal dangerous emissions. Smaller delivery parts in multi-generation cycles causes less costs and energy losses that can be considered as other benefits of a multi-generation power plant. The primary production of electricity is van be gotten from the nearest point to the users and from a centralized power plant. The efficiency drops about 9% because of the transmission and distribution from the base plant to the city [9]. The mentioned points and benefits of the multi-generation energy systems encourage the scientists and designer to step more in this field to solve the vague aspects. This higher overall energy efficiency apart from exergy efficiency is often the major factor in using multi-generation power plants. Before selecting any kind of multi-generation energy systems, additional assessments including calculation of initial capital and operation costs, is needed to guarantee efficient and economic multi-generation plant construction [8].

Geothermal water is one of the common renewable energy sources analyzed in details by researchers all around the world, which is capable to supply the sustainable and green energy for the needed demands. After finding the geothermal energy benefits and huge energy capacity, its usage has raised more than double as stated by several researchers [10]. The main limitation of using geothermal water energy is its different temperature by considering its location; so the needed temperature should be considered before choosing this type of energy source for the utilities.

There are three types of geothermal energy sources that are low temperature geothermal source (below 90°C), moderate temperature geothermal source (90–150°C) and high temperature geothermal source (above 150°C) [11]. Moderate-temperature geothermal energy source can supply the needed thermal energy to drive the Organic Rankine cycles, or they can be used to provide the needed heating and cooling using in absorption cooling equipment. The low-temperature geothermal energy source is the most suitable one as a direct heating source [12].

Useful and efficient ways to use geothermal sources has become so popular among the researchers and many articles have been published related to these interesting topics [13-15].

For those moderate and low temperature geothermal energy sources, it is much more suitable to use them directly for the heating and cooling purpose. Nevertheless, combination of the heat and power production from any kind of energy sources is always useful and helpful [16-18]. Combination of the heat and power (CHP) system is capable to produce both thermal energy and electricity generally in the shape of steam or hot water, and electricity [19].

1.4 Aims and Objectives

The novelty of this master thesis is to largely model and analyze a geo-thermal based multi-generation energy system by engineering equation Solver software (EES). In addition, energy, exergy and environmental impact assessment are conducted to improve the performance analysis of the system. In this study, a geothermal power plant integrated with TEAS, electrolyzer, and organic Rankine cycle is considered

for cooling, heating, hot water, hydrogen, and power production. This master research thesis is including of some main objects as below:

a) To extend the mathematical model for the designed multi-generation energy system:

Complete thermodynamic modeling of a multi-generation system integrated to geothermal energy as initial energy resource, an electrolyzer device to produce hydrogen production, a triple effect absorption chiller, dehumidification system and an organic Rankine cycle.

b) To achieve the exergy analysis of each multi-generation subsystem:

- Exergy analysis of the stream flow rate in each subsystem
- Calculation of the exergy destruction rate and exergy efficiency for the components.

c) To determine the system in aspect of its harmful effects on the environment and atmosphere

- Determination of environmental sustainability index (the system harmful effect on the environment) and finding the relation between exergy and environmental impacts.

d) To perform a complete parametric study and the performance assessment of the system.

- determination of a separate parametric study for each subsystem to achieve the effect of design parameter on the system performance such as environmental impacts and exergy efficiency.
- Effect of environment condition on the performance assessment of each subsystem.

Chapter 2

LITERATURE REVIEW

2.1 Introduction

In this section, a comprehensive study of the power plants using multi-generation energy system is illustrated. In addition, the various studies related to the CHPs and tri-generation energy systems are presented in this literature. In this chapter, a brief of the related papers including their methods of analyzing and their studies are presented. In addition, it is tried to cover the recent studies done by the researchers related to the multi-generation, tri-generation and cogeneration energy systems. The literature has been divided to the some parts depends on the thermodynamic modeling, energy, exergy of all the types of energy systems including cogeneration, tri-generation and multi-generation. The literature starts with the literature details then provides a view about recent related studies.

Recently, due to environmental concerns because of using fossil fuels in the power plants, defining new techniques to produce multiple outputs from a constant prime source has been become so popular by the governments. Utilities with multiple outputs can be defined to be capable to produce several outputs from the single or multiple energy inputs. The aim to design a multi-generation energy system is to increase the energy and exergy efficiency of the utility and decrease the environmental impacts at the same time. A multi-generation energy system can produce electricity, heating, cooling, hot water, hydrogen and dry air by the

dehumidification system. In a more simple way, cogeneration energy systems (combined heat and power) provide two products including thermal energy and electricity power. CHP energy cycles efficiency can be found from dividing the injected energy to the system by both cycle production (heats and electricity) and it is generally around 40-50% or higher in some cases [8].

Huangfu et al. [20] studied a stand-alone energy system for the building needs such as thermal energy, cooling load and electricity integrated to an absorption system as an experimental case. They analyzed the absorption chiller performance under different heating conditions. The authors could prove that there is a linear relation between the injected hot water temperature and absorption system for the two different systems. In a commercial case, CHP-ORC systems analyzed and optimized by Mago et al. [21]. As a residential case, an integrated CHP system with the storage capacity of the thermal and electric energy, studied by Bianchi et al. [22]. Energy efficiency evaluation and energy saving methods analyzed to solve the vague problems of energy efficiency for a combined cold, heat and electricity production system done by Havelsky [23].

Heat pumps was experimented to analyze the energy performance of a tri-generation utility by Miguez et al. [24-25]. This study could prove, heat pumps can increase the energy efficiency of the system.

Khaliq et al. [7] analyzed a system including refrigeration cycle and electricity in aspect of exergy performance and did a comprehensive analysis to determine the result of pitch point, gas type and exhaust gas inlet temperature on electricity, exergy destruction rate and energy-exergy efficiency for a combined cogeneration system.

In a case study located in Turkey, Cihan et al. [26] analyzed energy and exergy performance of a combined energy system to reduce the exergy destruction for a CHP. The proposed study could show that main part of the exergy destruction (near to 85%) is directly related to the gas turbine, heat recovery steam generators (HRSGs) and combustion chamber.

A Proton Exchange Membrane (PEM) fuel cell is considered to find the exergy analysis result for a residential CHP by Barelli et al. [27]. They also could achieve to the comprehensive inclusive study to find out results of fuel cell parameters including specific humidity, temperature and pressure on the system. A suitable high efficiency multi-generation system for the residential application was exergetic analyzed by Bingol et al. [28].

Both energetic and exergetic analysis of CHP energy cycle using fuel cell device and a gas turbine is done by El-emam and Dincer [29]. To reach the suitable system performance, they did comprehensive simulation to check the system by varying some major and effective factors. The analysis results showed that molten carbonate fuel cell (MCFC) systems could reach to the 3.14 kW as the maximum output power at the operation temperature range of 600-650°C. The total energy and exergy efficiencies can reach to 42.89% and 37.75%, respectively. A complete parametric study and hybrid CHP (using SOFC) linked to gas turbine is done by Akkaya et al. [30]. It is achieved from their results that entropy generation rate is affected by the exergy performance coefficient of the system. Al-sulaiman et al. [31] showed that the efficiency can be increased up to 22% by using tri-generation energy system integrated with an energy cycle.

They could prove that maximum efficiency for the tri-generation energy system, heating cogeneration system, cooling cogeneration system and net electricity generation can reach to 74%, 70%, 57% and 46%, respectively. In addition, they presented that exergy analysis is a power tool to determine the maximum power of the CHP or tri-generation energy systems.

2.2 Tri-generation Systems

The tri-generation systems are capable to produce electricity, heating and cooling with the same initial input energy source. The overall efficiency can be improved by using the waste heat of the power plant and free energy can be obtained for the waste energy. In these energy systems, the heating and cooling equipment can be driven by using the waste thermal energy released from prime movers [6]. The produced heat can be used for heating needs, steam producing and to heat the domestic water sources. The output heat also can be used to run the absorption system for air conditioning purpose. Popisisl et al. [32] did the comparative study for the mention energy systems and checked their results for a residential application. The results achieved to the point that cogeneration energy systems can increase the overall energy efficiency of a single generation system up to 31% while tri-generation system can raise the efficiency up to 39% in the same initial conditions. Three types of tri-generation systems including solar-trigeneration, Solfi oxide fuel cell (SOFC)-tri-generation and biomass-trigeneration were compared by Al-sulaiman et al. [33].

Influence of the main parameters on the thermodynamic performance of tri-generation energy systems analyzed by Martins et al. [34]. A planning parameter" equivalent gas price" defined by Chicco and mancarella [35] by installing some especial energy sensors to check the fuel heating value and efficiency of the energy

systems. Thermodynamic assessment on a tri-generation energy system done by Minciuc et al. [36] to define a new model for evaluating the system and find the limitations to link a gas turbine to reach the maximum performance.

Buck and Fredmann [37] analyzed system working results of a tri-generation energy system including a small-size solar energy system and a micro turbine. They showed that in a comparative study of single and double effect absorption system, in term or economics points, using double effect absorption system is more suitable because it can work in higher energy efficiency with the lower operation and maintenance expenses.

Exergy analysis is a helpful and powerful tool to determine the type and location of the exergy losses which can occur in the form of exergy destruction or emitted waste exergy [38]. Therefore, exergy analysis can show the best way to design and define the needed strategies for the energy system development. Recently, exergy has become more and more popular to assess the energy and thermal systems. Khaliq [39] analyzed the tri-generation energy system in term of exergy. The considered system is including an absorption system (single effect) to generate cooling loads, turbine, and primary heat recovery steam generator to supply the thermal energy. In addition, he did a complete parametric study to check the main parameter effects on the system performance. The results showed that combustion chamber and steam generator are the most important factors for the exergy destruction that cause high rate of exergy destruction in the system performance. Ahmadi et al. [6] showed an exergoenvironmental assessment of a tri-generation energy system connected to a gas turbine and organic Rankine cycle (ORC), and did a complete parametric study including the major factors in the tri-generation system.

Mago and Hueffed [40] analyzed a combined cooling; heating and power (CCHP) energy system linked to a turbine as a commercial office application and varies the operation parameters to find the amount of Carbon emission to calculate the Carbone reduction in using the CCHP energy systems. Many publications are available considering the environmental assessments of the energy systems. A hydrogen and fuel cell system are examined in term of environmental and sustainability points by Dincer [41], and Dincer and Rosen [38]. In addition, environmental evaluation of a dehumidification system is conducted [42].

2.3 Multi-generation Energy Cycles

This kind of system is defined as an energy cycle to produce multiple different outputs in comparison with tri-generation systems. It can generate heating, cooling, hydrogen, hot water electricity and dried air by the same initial energy injection. It is crucial to design these systems for the places with the high rate of demands such as residential areas, power plants, hotels, etc. as the most important factor to design a multi-generation energy system is to consider the enough construction area.

Hosseini et al. [43] designed and analyzed thermodynamically an integrated multi-generation system. The system is including of multi effect desalination, a primary heat recovery steam generator (HRSG) and a gas turbine to generate fresh water, thermal energy, cooling loads and electricity. This study also conducted an inclusive analysis was done to check the main parameters results on the system performance. They could also indicate that integrating energy cycles can raise the overall efficiency up to 25%.

A novel simulation of a tri-generation utility including of an organic Rankine cycle, a single effect absorption system, a gas turbine and recovery steam generator (double pressure) analyzed by Ahmadi et al. [6]. They presented a complete study analysis to check the results of the main factors on the system. The outputs of the study indicated that cycle performance is significantly affect by the gas turbine isentropic efficiency, turbine inlet temperature and compressor pressure ratio.

An integrated photovoltaic thermal (PV/T) and absorption system to produce hydrogen and cooling production studied by Ratlamwala et al. [44]. In addition, parametric study was done on the different electrolyzer working hour, sun irradiations, PV area and inlet air temperature on the hydrogen and power production.

Ratlamwala et al. [45] studied a novel simulation on a multi-generation energy cycle using geothermal as inlet energy source linked to double flash power generating unit and using ammonia/water as the working fluid, absorption system and electrolyzer. Output power, hydrogen production can be increased by raising the inlet geothermal temperature, mass flow and pressure. A solar-based multi-generation cycle with hydrogen production including of electrolyzer, ORC, absorption chiller, designed and analyzed by Ozturk and Dincer [46]. The results showed that using parabolic trough dishes has the highest rate of exergy destruction in comparison with other types (lower overall exergy efficiency).

Dincer and Zamfirescu [7] presented a complete energy and exergy analysis of a renewable-energy-based multi-generation system to produce hydrogen, cooling, heating, hot water, electricity and dried air. The scientists and researchers

recommend that using integrated multi-generation (especially energy systems integrated to renewable sources) can be useful to come up with a solution to increase the overall energy and exergy efficiency of the energy systems and decrease the environmental impacts to save the nature and its creatures.

Chapter 3

DESCRIPTION OF THE SYSTEM

The system including integrated triple effect LiBr/water absorption with organic Rankine cycle, an electrolyzer, and an air conditioning system, which is presented in the current research, is illustrated in Figure 3.1. The proposed energy system is capable to generate six valuable productions, namely electricity (power), thermal energy, hot water, cooling loads, hydrogen and conditioned air (dry air). A geothermal energy source is selected to as the energy carrier of the system by going over the TEAS to generate heating, cooling, and hot water, as presented in Figure 3.1.

Total heating and cooling production (by TEAS) are then tansported to the residential areas. The exiting geothermal water from TEAS then will pass through the solar collector to increase its temperature at state 29 and will enter the ORC boiler to vaporize the ammonia to produce power for the hydrogen production unit besides the buildings. It should be noted that the cold level of the sea has been used to decrease the condenser temperature in organic Rankine cycle (ORC) at state 38. After that, the geothermal water will leave the boiler at state 31 and will supply the domestic hot water for the buildings.

The cooling production is separated into two parts. One share is provided for domestic purposes of the buildings, and the other portion is sent for the air-

conditioning devices to deliver chilled and dried air to cold loadings. The produced hydrogen is kept in the tank chambers and can be used advanced as the needed amount by the consumer. As shown in Figure 3.1, the air conditioning system that is measured in the current thesis is cooling load through dehumidification for supplying cooled dry air. The humid air flows to the dehumidification system at state 41, passes into the cooling coil where it meets cooled coils. The cooled coils condense the humid air and help it in losing wetness. Then dried and conditioned air leaves the system to supply in the dry cold tanks.

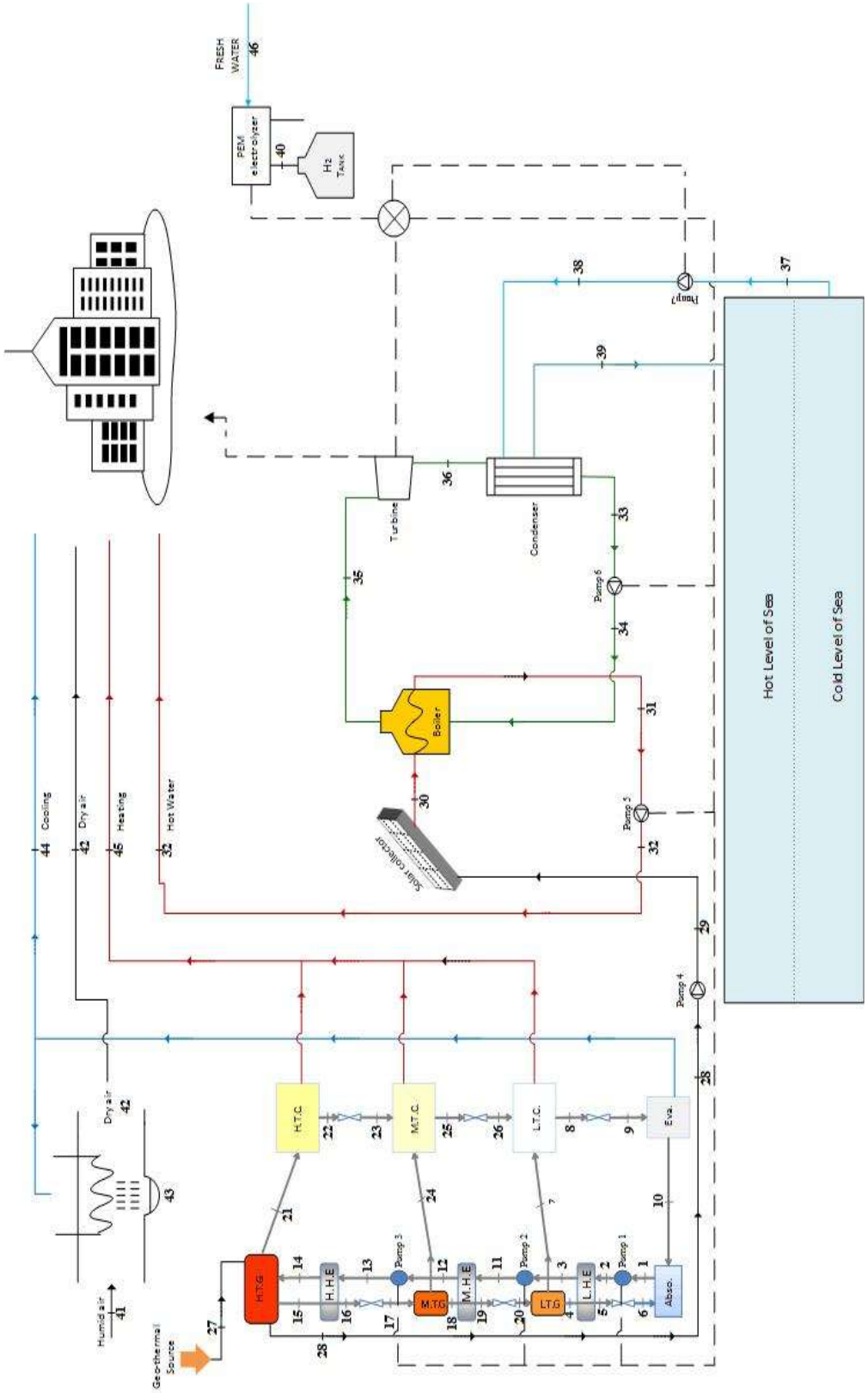

Figure 3.1: Multi-generation system

Chapter 4

MODEL DEVELOPMENT AND ANALYSIS

4.1 Thermodynamic Analysis

To examine the proposed integrated system, energetic and exergetic analyzes were considered. The energy, exergy, and mass balance equations are written for each component of TEAS and the ammonia Rankine thermodynamic cycle. Also, the efficiency of the Rankine cycle and COPs of TEAS equations are calculated. The system is assumed to be working under thermodynamic steady state conditions. Heat loss and pressure drops in heat exchangers and the connecting piping system are also considered negligible. Moreover, the parasitic losses (from the solar collectors) produced by the pumps and turbines are measured in calculating the net power output from the plant. Finally, the heat exchangers are modeled on the principle of temperature change and for each heat exchange of TEAS, the temperature change is considered constant.

In addition, by calculating and considering the exergy efficacy and exergy destruction, the exergoenvironmental analysis can be obtained to analyze their impacts on the environments. This analysis is including of six main parameters that are listed as below.

4.1.1 Exergoenvironmental Impact Factor

The exergoenvironmental impact factor determines the positive effect of the investigated system on the environment. The purpose of studying this parameter is that it helps in reducing the environmental impact of the system by decreasing the irreversibilities in the system.

4.1.2 Exergoenvironmental Impact Coefficient

The exergoenvironmental impact coefficient is related to the exergetic efficiency of the system.

4.1.3 Exergoenvironmental Impact Index

The exergoenvironmental impact index is an important parameter to study as it indicates whether the system under investigation damages the environment due to its unusable waste exergy output and exergy destruction.

4.1.4 Exergoenvironmental Impact Improvement

The exergoenvironmental impact improvement parameter helps finding the environmental appropriateness of the investigated system.

4.1.5 Exergetic Stability Factor

The exergetic stability factor is a function of the desired output exergy, total exergy destruction, and exergy carried by unused fuel.

4.1.6 Exergetic Sustainability Index

The exergetic sustainability index is the multiplication of exergetic stability factor and exergoenvironmental impact improvement of the system.

4.2 Equations

Energy, Exergy Analyzes and Environmental Impacts Assessment are illustrated below.

4.2.1 Absorber Analysis

Figure 4.1 illustrates schematic of the absorber. (Also, see Figure 3.1).

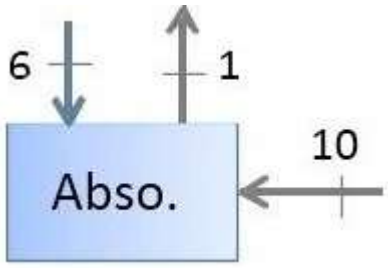

Figure 4.1: Schematic of the absorber

The following equations are used for the absorber.

$$\dot{Q}_{Abs} = \dot{m}_1 * h_1 + \dot{m}_{10} * h_{10} + \dot{m}_6 * h_6 \quad (1)$$

$$\dot{E}x_{q,\mathrm{Abs}} = (1 - T_0 / T_{avg}) * \dot{Q}_{Abs} \quad (2)$$

$$T_{avg} = (T_1 + T_6 + T_{10}) / 3 \quad (3)$$

$$\dot{E}x_{d,Abs} = \dot{E}x_{10} + \dot{E}x_6 - \dot{E}x_1 - \dot{E}x_{q,\mathrm{Abs}} \quad (4)$$

Where $\dot{Q}_{Abs}$, $\dot{m}_i$, $\dot{E}x_{q,\mathrm{Abs}}$, T_0, T_{avg}, $\dot{E}x_{d,Abs}$ and $\dot{E}x_i$ presents absorber heat flow rate, mass flow, thermal exergy rate, ambient temperature, average temperature, exergy destruction rate, and sate exergy rate , respectively.

4.2.2 Low Temperature Heat exchanger Analysis

Figure 4.2 illustrates schematic of the low temperature heat exchanger. (Also, see Figure 3.1)

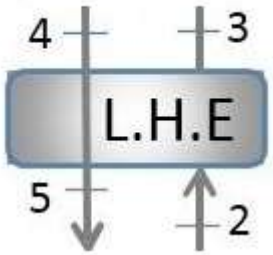

Figure 4.2: Schematic of the low temperature heat exchanger

The following equations are used for the low temperature heat exchanger.

$$\dot{Q}_{LHE} = \dot{m}_4 * \mathrm{h}_4 - \dot{\mathrm{m}}_5 * \mathrm{h}_5 \tag{5}$$

$$\dot{E}x_{q,\mathrm{LHE}} = (1 - T_0 / T_{avg}) * \dot{Q}_{LEH} \tag{6}$$

$$T_{avg} = (T_4 + T_2 + T_3 + T_5) / 4 \tag{7}$$

$$\dot{E}x_{d,\mathrm{LHE}} = \dot{E}x_2 + \dot{E}x_4 - \dot{E}x_5 - \dot{E}x_{q,\mathrm{LHE}} - \dot{E}x_3 \tag{8}$$

Where $\dot{Q}_{LHE}$, $\dot{m}_i$, $\dot{E}x_{q,\mathrm{LHE}}$, T_0, T_{avg}, $\dot{E}x_{d,\mathrm{LHE}}$ and $\dot{E}x_i$ presents low temperature heat exchanger heat flow rate, mass flow, thermal exergy rate, ambient temperature, average temperature, exergy destruction rate, and sate exergy rate , respectively.

4.2.3 Pump 1 Analysis

Figure 4.3 illustrates schematic of the pump 1. (Also, see Figure 3.1)

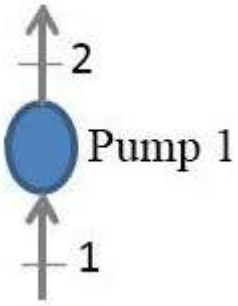

Figure 4.3: Schematic of the pump 1

The following equations are used for the pump 1.

$$\dot{W}_{pump,1} = (\dot{m}_1 * v_1 * (P_2 - P_1)) / \eta_{\text{isentropic}} \quad (9)$$

$$\dot{E}x_1 + \dot{W}_{pump,1} = \dot{E}x_2 + \dot{E}x_{d,pump,1} \quad (10)$$

Where $\dot{W}_{pump,1}$, $\dot{m}_i$, v_1, P_2, $\eta_{\text{isentropic}}$, $\dot{E}x_{d,pump1}$ and $\dot{E}x_i$ present pump work, mass flow, specific volume, pressure, isentropci efficency, exergy destruction rate and sate exergy rate , respectively.

4.2.4 Low Temperature Generator Analysis

Figure 4.4 illustrates schematic of the low temperature generator. (Also, see Figure 3.1)

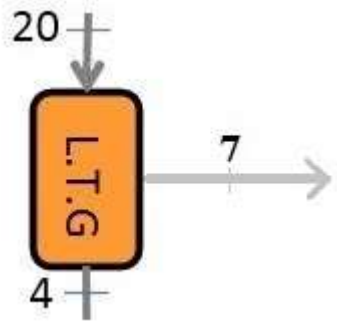

Figure 4.4: Schematic of the low temperature generator

The following equations are used for the low temperature generator.

$$\dot{Q}_{LTG} = -\dot{m}_4 * \mathrm{h}_4 + \dot{\mathrm{m}}_{20} * \mathrm{h}_{20} - \dot{\mathrm{m}}_7 * \mathrm{h}_7 \quad (11)$$

$$\dot{E}x_{q,\mathrm{LTG}} = (1 - T_0 / T_{avg}) * \dot{Q}_{LTG} \quad (12)$$

$$T_{avg} = (T_4 + T_{20} + \mathrm{T}_7) / 3 \quad (13)$$

$$\dot{E}x_{d,Abs} = \dot{E}x_{20} - \dot{E}x_4 + \dot{E}x_{q,\mathrm{LTG}} - \dot{E}x_7 \quad (14)$$

Where $\dot{Q}_{LTG}$, $\dot{m}_i$, $\dot{E}x_{q,\mathrm{LTG}}$, T_0, T_{avg}, $\dot{E}x_{d,\mathrm{LTG}}$ and $\dot{E}x_i$ presents low temperature generator heat flow rate, mass flow, thermal exergy rate, ambient temperature, average temperature, exergy destruction rate, and sate exergy rate , respectively.

4.2.5 Pump 2 Analysis

Figure 4.5 illustrates schematic of the pump 2. (Also, see Figure 3.1)

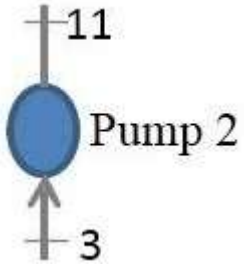

Figure 4.5: Schematic of the pump 2

The following equations are used for the pump 2.

$$\dot{W}_{pump,2} = (\dot{m}_3 * v_3 * (P_{11} - P_3)) / \eta_{\text{isentropic}} \quad (15)$$

$$\dot{E}x_3 + \dot{W}_{pump,2} = \dot{E}x_{11} + \dot{E}x_{d,pump,2} \quad (16)$$

Where $\dot{W}_{pump,2}$, $\dot{m}_i$, v_3, P_i, $\eta_{\text{isentropic}}$, $\dot{E}x_{d,pump2}$ and $\dot{E}x_i$ present pump work, mass flow, specific volume, pressure, isentropic efficieny, exergy destruction rate and sate exergy rate , respectively.

4.2.6 Moderate Temperature Heat Exchanger Analysis

Figure 4.6 illustrates schematic of the moderate temperature heat exchanger. (Also, see Figure 3.1)

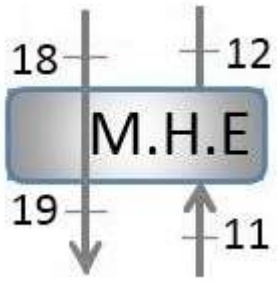

Figure 4.6: Schematic of the moderate temperature heat exchanger

The following equation are used for the moderate temperature heat exchanger.

$$\dot{Q}_{MHE} = -\dot{m}_{19} * \mathrm{h}_{19} + \dot{\mathrm{m}}_{18} * \mathrm{h}_{18} \tag{17}$$

$$\dot{E}x_{q,\mathrm{MHE}} = (1 - T_0 / T_{avg}) * \dot{Q}_{MHE} \tag{18}$$

$$T_{avg} = (T_{18} + T_{11} + T_{12} + T_{19}) / 4 \tag{19}$$

$$\dot{E}x_{d,\mathrm{MHE}} = -\dot{E}x_{11} - \dot{E}x_{18} + \dot{E}x_{12} - \dot{E}x_{q,\mathrm{MHE}} + \dot{E}x_{19} \tag{20}$$

Where $\dot{Q}_{MHE}$, $\dot{m}_i$, $\dot{E}x_{q,\mathrm{MHE}}$, T_0, T_{avg}, $\dot{E}x_{d,\mathrm{MHE}}$ and $\dot{E}x_i$ present moderate temperature heat exchanger heat flow rate, mass flow, thermal exergy rate, ambient temperature, average temperature, exergy destruction rate, and sate exergy rate , respectively.

4.2.7 Moderate Temperature Generator Analysis

Figure 4.7 illustrates schematic of the moderate temperature generator. (Also, see Figure 3.1)

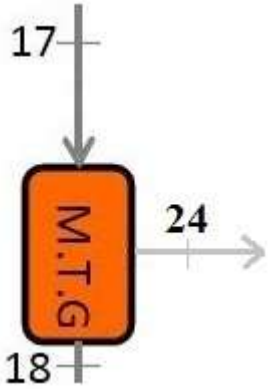

Figure 4.7: Schematic of the moderate temperature generator

The following equation are used for the moderate temperature generator.

$$\dot{Q}_{MTG} = \dot{m}_{24} * \mathrm{h}_{24} - \dot{\mathrm{m}}_{17} * \mathrm{h}_{17} + \dot{m}_{18} * \mathrm{h}_{18} \quad (21)$$

$$\dot{E}x_{q,\mathrm{MTG}} = (1 - T_0 / T_{avg}) * \dot{Q}_{MTG} \quad (22)$$

$$T_{avg} = (T_{18} + T_{17} + T_{24}) / 3 \quad (23)$$

$$\dot{E}x_{d,\mathrm{MTG}} = \dot{E}x_{17} - \dot{E}x_{24} + \dot{E}x_{q,\mathrm{MTG}} - \dot{E}x_{18} \quad (24)$$

Where $\dot{Q}_{MTG}$, $\dot{m}_i$, $\dot{E}x_{q,\mathrm{MTG}}$, T_0, T_{avg}, $\dot{E}x_{d,\mathrm{MTG}}$ and $\dot{E}x_i$ present moderate temperature generator heat flow rate, mass flow, thermal exergy rate, ambient temperature, average temperature, exergy destruction rate, and sate exergy rate , respectively.

4.2.8 Pump 3 Analysis

Figure 4.8 illustrates schematic of the pump 3. (Also, see Figure 3.1)

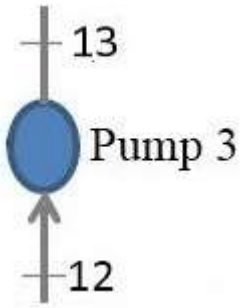

Figure 4.8 illustrates schematic of the pump 3

The following equations are used for the pump 3.

$$\dot{W}_{pump,3} = (\dot{m}_{12} * v_{12} * (P_{13} - P_{12})) / \eta_{\text{isentropic}} \quad (25)$$

$$\dot{E}x_{12} + \dot{W}_{pump,3} = \dot{E}x_{13} + \dot{E}x_{d,pump,3} \quad (26)$$

Where $\dot{W}_{pump,3}$, $\dot{m}_i$, v_{12}, P_i, $\eta_{\text{isentropic}}$, $\dot{E}x_{d,pump3}$ and $\dot{E}x_i$ present pump work, mass flow, specific volume, pressure, isentropic efficiency, exergy destruction rate and sate exergy rate , respectively.

4.2.9 High Temperature Heat Exchanger Analysis

Figure 4.9 illustrates schematic of the high temperature heat exchanger. (Also, see Figure 3.1)

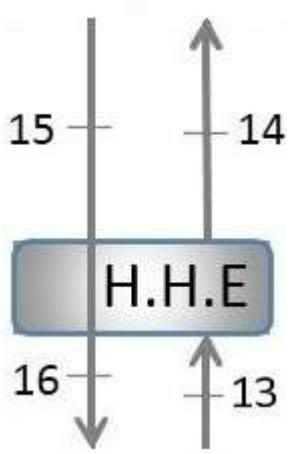

Figure 4.9: Schematic of the high temperature heat exchanger

The following equations are used for the high temperature heat exchanger.

$$\dot{Q}_{HHE} = \dot{m}_{15} * \mathrm{h}_{15} - \dot{\mathrm{m}}_{16} * \mathrm{h}_{16} \tag{27}$$

$$\dot{E}x_{q,\mathrm{HHE}} = (1 - T_0 / T_{avg}) * \dot{Q}_{HHE} \tag{28}$$

$$T_{avg} = (T_{14} + T_{15} + T_{12} + T_{16}) / 4 \tag{29}$$

$$\dot{E}x_{d,\mathrm{HHE}} = \dot{E}x_{12} + \dot{E}x_{15} - \dot{E}x_{14} + \dot{E}x_{q,\mathrm{HEE}} - \dot{E}x_{16} \tag{30}$$

Where $\dot{Q}_{HHE}$, $\dot{m}_i$, $\dot{E}x_{q,\mathrm{HHE}}$, T_0, T_{avg}, $\dot{E}x_{d,\mathrm{HHE}}$ and $\dot{E}x_i$ presents high temperature heat exchanger heat flow rate, mass flow, thermal exergy rate, ambient temperature, average temperature, exergy destruction rate, and sate exergy rate , respectively.

4.2.10 High Temperature Generator Analysis

Figure 4.10 illustrates schematic of the high temperature generator. (Also, see Figure 3.1)

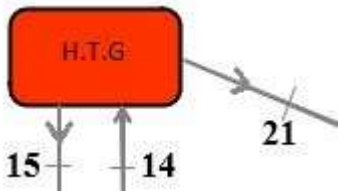

Figure 4.10: Schematic of the high temperature generator

The following equations are used for the high temperature generator.

$$\dot{Q}_{HTG} = \dot{m}_{27} * \mathrm{c}_{\mathrm{p},27}(\mathrm{T}_{27} - \mathrm{T}_{28}) \tag{31}$$

$$\dot{E}x_{q,\mathrm{HTG}} = (1 - T_0 / T_{avg}) * \dot{Q}_{HTG} \tag{32}$$

$$T_{avg} = (T_{14} + T_{15} + T_{21}) / 3 \tag{33}$$

$$\dot{E}x_{d,\mathrm{HTG}} = \dot{E}x_{14} - \dot{E}x_{15} - \dot{E}x_{21} + \dot{E}x_{q,\mathrm{HTG}} \tag{34}$$

Where $\dot{Q}_{HTG}$, $\dot{m}_i$, $\dot{E}x_{q,\mathrm{HTG}}$, T_0, T_{avg}, $\dot{E}x_{d,\mathrm{HTG}}$ and $\dot{E}x_i$ present high temperature generator heat flow rate, mass flow, thermal exergy rate, ambient temperature, average temperature, exergy destruction rate, and sate exergy rate , respectively.

4.2.11 High Temperature Condenser Analysis

Figure 4.11 illustrates schematic of the high temperature condenser. (Also, see Figure 3.1)

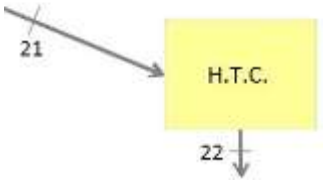

Figure 4.11: Schematic of the high temperature condenser

The following equations are used for high temperature condenser.

$$\dot{Q}_{HTC} = \dot{m}_{21} * \mathrm{h}_{21} - \dot{\mathrm{m}}_{22} * \mathrm{h}_{22} \quad (35)$$

$$\dot{E}x_{q,\mathrm{HTC}} = (1 - T_0 / T_{avg}) * \dot{Q}_{HTC} \quad (36)$$

$$T_{avg} = (T_{21} + T_{22}) / 2 \quad (37)$$

$$\dot{E}x_{d,\mathrm{HTC}} = \dot{E}x_{21} - \dot{E}x_{22} + \dot{E}x_{q,\mathrm{HEE}} \quad (38)$$

Where $\dot{Q}_{HTC}$, $\dot{m}_i$, $\dot{E}x_{q,\mathrm{HTC}}$, T_0, T_{avg}, $\dot{E}x_{d,\mathrm{HTC}}$ and $\dot{E}x_i$ present high temperature condenser heat flow rate, mass flow, thermal exergy rate, ambient temperature, average temperature, exergy destruction rate, and sate exergy rate , respectively.

4.2.12 Moderate Temperature Condenser Analysis

Figure 4.12 illustrates schematic of the moderate temperature condenser. (Also, see Figure 3.1)

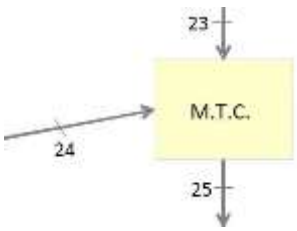

Figure 4.12: Schematic of the moderate temperature condenser

The following equations are used for moderate temperature condenser.

$$\dot{Q}_{MTC} = \dot{m}_{24} * \mathrm{h}_{24} + \dot{\mathrm{m}}_{23} * \mathrm{h}_{23} - \dot{\mathrm{m}}_{25} * \mathrm{h}_{25} \quad (39)$$

$$\dot{E}x_{q,\mathrm{MTC}} = (1 - T_0 / T_{avg}) * \dot{Q}_{MTC} \quad (40)$$

$$T_{avg} = (T_{24} + T_{23} + T_{25}) / 3 \quad (41)$$

$$\dot{E}x_{d,\mathrm{MTC}} = \dot{E}x_{23} + \dot{E}x_{24} + \dot{E}x_{q,\mathrm{HEE}} - \dot{E}x_{25} \quad (42)$$

Where $\dot{Q}_{MTC}$, $\dot{m}_i$, $\dot{E}x_{q,\mathrm{MTC}}$, T_0, T_{avg}, $\dot{E}x_{d,\mathrm{MTC}}$ and $\dot{E}x_i$ present moderate temperature condenser heat flow rate, mass flow, thermal exergy rate, ambient temperature, average temperature, exergy destruction rate, and sate exergy rate , respectively.

4.2.13 Low Temperature Condenser Analysis

Figure 4.13 illustrates schematic of the low temperature condenser. (Also, see Figure 3.1)

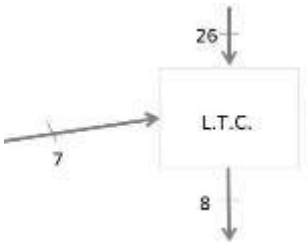

Figure 4.13: Schematic of the low temperature condenser

The following equations are used for low temperature condenser.

$$\dot{Q}_{COND} = \dot{m}_{26} * \mathrm{h}_{26} + \dot{\mathrm{m}}_7 * \mathrm{h}_7 - \dot{\mathrm{m}}_8 * \mathrm{h}_8 \tag{43}$$

$$\dot{E}x_{q,COND} = (1 - T_0 / T_{avg}) * \dot{Q}_{COND} \tag{44}$$

$$T_{avg} = (T_8 + T_{26} + T_7) / 3 \tag{45}$$

$$\dot{E}x_{d,\mathrm{COND}} = \dot{E}x_7 + \dot{E}x_{26} + \dot{E}x_{q,\mathrm{HEE}} - \dot{E}x_8 \tag{46}$$

Where $\dot{Q}_{COND}$, $\dot{m}_i$, $\dot{E}x_{q,\mathrm{COND}}$, T_0, T_{avg}, $\dot{E}x_{d,\mathrm{COND}}$ and $\dot{E}x_i$ present low temperature condenser heat flow rate, mass flow, thermal exergy rate, ambient temperature, average temperature, exergy destruction rate, and sate exergy rate , respectively.

4.2.14 Evaporator Analysis

Figure 4.14 illustrates schematic of the evaporator. (Also, see Figure 3.1)

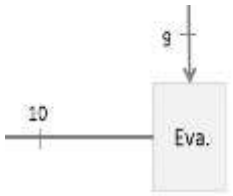

Figure 4.14: Schematic of the evaporator

The following equations are used for the evaporator.

$$\dot{Q}_{EVAP} = \dot{m}_{10} * \mathrm{h}_{10} - \dot{\mathrm{m}}_9 * \mathrm{h}_9 \tag{47}$$

$$\dot{E}x_{q,\mathrm{EVAP}} = (1 - T_0 / T_{avg}) * \dot{Q}_{EVAP} \tag{48}$$

$$T_{avg} = (T_9 + T_{107}) / 2 \tag{49}$$

$$\dot{E}x_{d,\mathrm{EVAP}} = \dot{E}x_9 - \dot{E}x_{10} + \dot{E}x_{q,\mathrm{EVAP}} \tag{50}$$

Where $\dot{Q}_{EVAP}$, $\dot{m}_i$, $\dot{E}x_{q,\mathrm{EVAP}}$, T_0, T_{avg}, $\dot{E}x_{d,\mathrm{EVAP}}$ and $\dot{E}x_i$ present evaporator heat flow rate, mass flow, thermal exergy rate, ambient temperature, average temperature, exergy destruction rate, and sate exergy rate , respectively.

4.2.15 Turbine Analysis

Figure 4.15 illustrates schematic of the turbine. (Also, see Figure 3.1)

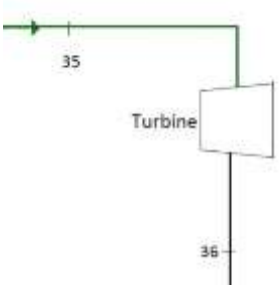

Figure 4.15: Schematic of the turbine

The following equations are used for the turbine.

$$\dot{W}_{Turbine} = (\dot{m}_{33} * (h_{35} - h_{36})) / \eta_{\text{isentropic}} \quad (51)$$

$$\dot{E}x_{d,pump,3} = \dot{E}x_{35} - \dot{W}_{Turbine} - \dot{E}x_{36} \quad (52)$$

Where $\dot{W}_{Turbine}$, $\dot{m}_i$, h_i, $\eta_{\text{isentropic}}$, $\dot{E}x_{d,\text{turbine}}$ and $\dot{E}x_i$ present turbine net work, mass flow, enthalpy, isentropic efficiency, exergy destruction rate, and sate exergy rate , respectively.

4.2.16 Condenser Analysis

Figure 4.16 illustrates schematic of the condenser. (Also, see Figure 3.1)

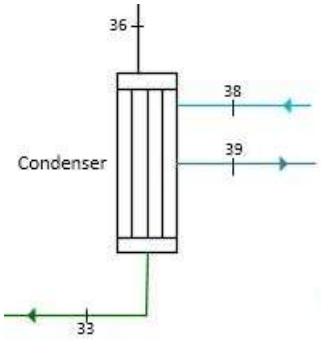

Figure 16: Schematic of the condenser

The following equations are used for the condenser.

$$\dot{Q}_{outcond} = \dot{m}_{36} * (\mathrm{h}_{36} - \mathrm{h}_{33}) \quad (23)$$

$$\dot{E}x_{q,\text{condrankine}} = (1 - T_0 / T_{avg}) * \dot{Q}_{outcond} \quad (54)$$

$$T_{avg} = (T_{36} + T_{33} + T_{38} + T_{39}) / 4 \quad (55)$$

$$\dot{E}x_{d,\text{condrankine}} = \dot{E}x_{36} + \dot{E}x_{38} + \dot{E}x_{q,\text{condrankine}} - \dot{E}x_{39} \quad (56)$$

Where $\dot{Q}_{outcond}$, $\dot{m}_i$, $\dot{E}x_{q,\text{condrankine}}$, T_0, T_{avg}, $\dot{E}x_{d,\text{condrankine}}$, $\dot{E}x_i$ and h_i present condenser heat flow rate, mass flow, thermal exergy rate, ambient temperature,

average temperature, exergy destruction rate, sate exergy rate and enthalpy , respectively.

4.2.17 Pump 6 Analysis

Figure 4.17 illustrates schematic of the pump 6. (Also, see Figure 3.1)

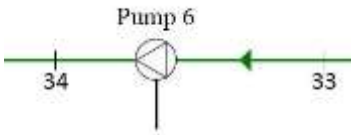

Figure 4.17: Schematic of the pump 6

The following equations are used for the pump 6.

$$\dot{W}_{pump,6} = (\dot{m}_{33} * v_{33} * (P_{34} - P_{33})) / \eta_{isentropic} \quad (57)$$

$$\dot{E}x_{33} + \dot{W}_{pump,6} = \dot{E}x_{34} + \dot{E}x_{d,pump,6} \quad (58)$$

Where $\dot{W}_{pump,6}$, $\dot{m}_i$, v_{33}, P_i, $\eta_{isentropic}$, $\dot{E}x_{d,pump6}$ and $\dot{E}x_i$ presents pump work, mass flow, specific volume, pressure, isentropic efficiency, exergy destruction rate and sate exergy rate , respectively.

4.2.18 Boiler Analysis

Figure 4.18 illustrates schematic of the boiler. (Also, see Figure 3.1)

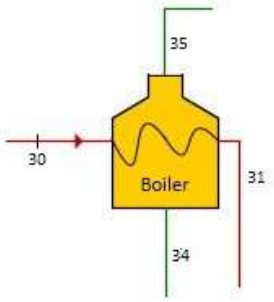

Figure 4.18: Schematic of the boiler

The following equations are used for the boiler.

$$\dot{Q}_{boil} = \dot{m}_{30} * \mathrm{h}_{30} - \dot{\mathrm{m}}_{31} * \mathrm{h}_{31} \tag{59}$$

$$\dot{E}x_{q,\mathrm{boil}} = (1 - T_0 / T_{avg}) * \dot{Q}_{boil} \tag{60}$$

$$T_{avg} = (T_{34} + T_{35} + T_{30} + T_{31}) / 4 \tag{61}$$

$$\dot{E}x_{d,\mathrm{boil}} = -\dot{E}x_{35} + \dot{E}x_{34} + \dot{E}x_{q,\mathrm{boil}} \tag{62}$$

Where $\dot{Q}_{boil}$, $\dot{m}_i$, $\dot{E}x_{q,\mathrm{boil}}$, T_0, T_{avg}, $\dot{E}x_{d,\mathrm{boil}}$ and $\dot{E}x_i$ present boiler heat flow rate, mass flow, thermal exergy rate, ambient temperature, average temperature, exergy destruction rate and sate exergy rate, respectively.

4.2.19 Electrolyzer Analysis

Figure 4.19 illustrates schematic of the electrolyzer. (Also, see Figure 3.1)

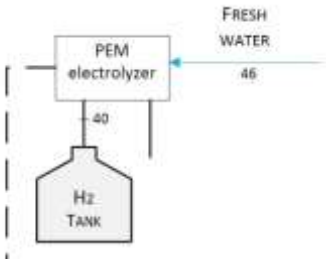

Figure 4.19: Schematic of the electrolyzer

The following equations are used for the electrolyzer.

$$\dot{m}_{h_2} = (\eta_{elec} * \dot{w}_{net}) / HHV \tag{63}$$

$$Ex_{phH_2} = (h_{40} - h_0) - T_0 * (s_{40} - s_0) \tag{64}$$

$$Ex_{chH_2} = (235.153 * 1000) / MW \tag{65}$$

$$\dot{E}x_{H_2} = \dot{m}_{H_2} (Ex_{phH2} + Ex_{chH2}) \tag{66}$$

$$\dot{E}x_{d,H_2} = Ex_{46} - Ex_{H_2} \quad (67)$$

Where $\dot{m}_{h_2}$, $\dot{m}_{H_2}$, η_{elec}, T_0, $\dot{w}_{net}$, HHV, Ex_{phH_2}, h_i, s_i, Ex_{chH_2}, MW, $\dot{E}x_{d,H_2}$ and $\dot{E}x_{H_2}$ present hydrogen production mass flow, water mass flow (entering to the electrolyzer), telectrolyzer efficeincy, ambient temperature, nelectrolyzer work, high heating valu, physical exergy, enthalpy, entropy, chemical exergy, molar mass, exergy destruction rate and sate exergy rate, respectively.

4.2.20 Dehumidification System Analysis

Figure 4.20 illustrates schematic of the dehumidification system. (Also, see Figure 3.1)

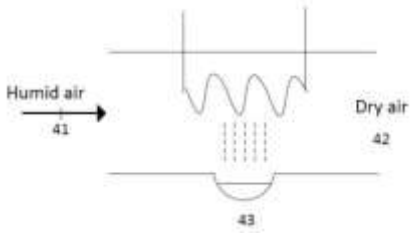

Figure 4.20: Schematic of the dehumidification system

The following equation are used for the dehumidification system.

$$\eta_{dehumidification} = (\dot{m}_{air\,42} * h_{42} / \dot{Q}_{dehumidification}) * 100 \quad (68)$$

$$\dot{m}_{air\,41} * w_{41} = \dot{m}_{air\,42} * w_{42} + \dot{m}_{water} \quad (69)$$

$$\dot{Q}_{dehumidification} = \dot{m}_{air\,42} * (h_{41} - h_{42}) - \dot{\mathrm{m}}_{\mathrm{water}} * \mathrm{h}_{\mathrm{water}} \quad (70)$$

$$\dot{E}x_{q,dehumidification} = (1 - T_0 / T_{avg}) * \dot{Q}_{dehumidification} \quad (71)$$

$$\dot{E}x_{d,dehumidification} = \dot{E}x_{41} - \dot{E}x_{42} - \dot{E}x_{43} - \dot{E}x_{q,dehumidification} \quad (72)$$

Where $\eta_{dehumidification}$, $\dot{m}_{air,i}$, h_i, T_0, $\dot{Q}_{dehumidification}$, w_i, $\dot{E}x_{q,dehumidification}$, T_{avg}, $\dot{E}x_{d,dehumidification}$ and $\dot{E}x_i$, present dehumidification system efficiency, air mass flow rate , enthalpy, ambient temperature, dehumidification heat flow rate, specific humidity, thermal exergy rate, average temperature, exergy destruction rate and sate exergy rate, respectively.

$$COP_{en} = (\dot{Q}_{eva} + \sum \dot{Q}_{cond}) / (\dot{Q}_{geo} + \sum \dot{W}_p) \tag{73}$$

$$COP_{ex} = (\dot{E}x_{q,eva} + \sum \dot{E}x_{q,cond}) / (\dot{E}x_{q,geo} + \sum \dot{W}_p) \tag{74}$$

In general, the efficiency of a primary Rankine cycle can be found as

$$\eta_{thermal} = (\dot{W}_{net} / \dot{Q}_{in}) * 100 \tag{75}$$

$$f_{ei} = \frac{\dot{E}x_{dest,tot}}{\sum \dot{E}x_{in}} \tag{76}$$

where f_{ei}, $\dot{E}x_{des,tot}$ and $\dot{E}x_{in}$ presents exergoenvironmental impact factor, total exergy destruction in the system and total exergy supplied to the system, respectively.

$$C_{ei} = \frac{1}{\frac{\eta_{ex}}{100}} \tag{77}$$

where C_{ei} and η_{ex} represent exergoenvironmental impact coefficient and exergetic efficiency, respectively.

$$\theta_{ei} = f_{ei} * C_{ei} \tag{78}$$

where θ_{ei} represents exergoenvironmental impact index.

$$\theta_{eii} = \frac{1}{\theta_{ei}} \tag{79}$$

where θ_{eii} represents exergoenvironmental impact improvement.

$$f_{es} = \frac{\dot{E}x_{tot,out}}{\dot{E}x_{tot,out} + \dot{E}x_{des,tot} + \dot{E}x_{uu}} \quad (80)$$

where f_{es} and $\dot{E}x_{uu}$ represent exergetic stability factor and exergy carried by unused fuel.

$$\theta_{est} = f_{es} * \theta_{eii} \quad (81)$$

where θ_{est} represent exergetic sustainability index.

Chapter 5

RESULTS AND DISCUSSIONS

5.1 Introduction

In recent decades, the environmental concerns due to high rate of fossil fuels usage, encourage researchers to find new alternative energy sources such as geothermal which is discussed as above.

In this paper, a system was designed which integrates geothermal power plant to supply heat for the system, TEAS and PEM electrolyzer for heating, cooling and hydrogen as well as an air conditioning system to produce dry air. The ambient temperature, evaporator temperature, geothermal water temperature and specific humidity were varied to investigate their effects on $\mathcal{E}_{en}$, $\mathcal{E}_{ex}$ COP_{en}, COP_{ex}, $\dot{V}_{H_2}$, net power, hot water, heat rate and dehumidification efficiency in the air conditioning system. To validate the results, absorption system was scaled down to match the system that was studied by [51], and obtained results are compared in Table 1. In addition, environmental assessment results are compared by a comprehensive parametric study, which is presented below.

Table 5.1: Evaluation of the current thesis results with the previous simulations done by other researchers.[47]

Related factors	This thesis	Previous studies[47]
$\dot{Q}_{geo}$	120 (kW)	120 (kW)
$\dot{Q}_{cond}$	90 (kW)	93 (kW)
$\dot{Q}_{eva}$	91 (kW)	91.55 (kW)
COP_{en}	0.7629	0.753

5.2 Obtained Results

5.2.1 Effect of Evaporator Temperature on COP_{en} and COP_{ex}

Evaporator temperature is one of the crucial parameters affecting both $\dot{Q}_{cooling}$ and system performance. By raising the evaporator temperature from 274K to 279K for all three amounts of mass flow, there is a downward trend for energetic and exergetic COP. By increasing the evaporator temperature, energetic COP will decline for all three varying mass flows from 1.491 to 1.479, 2.864 to 2.841 and 4.237 to 4.203, respectively for the mass flows of 0.1649, 0.3298 and 0.4947kg/s. There is also a decreasing trend for exergetic COP but it is more significant for energetic COP. By varying evaporator temperature from 274K to 279K, the COP_{ex} will fell from 0.3525 to 0.3145, 0.6359 to 0.5598 and 0.9194 to 0.8052 for the same three varying mass flows. By analyzing Figure 5.1, it is clear that by rising the evaporator temperature, the performance of the system will decrease so it is more desirable to keep the system in a cooler evaporator temperature.

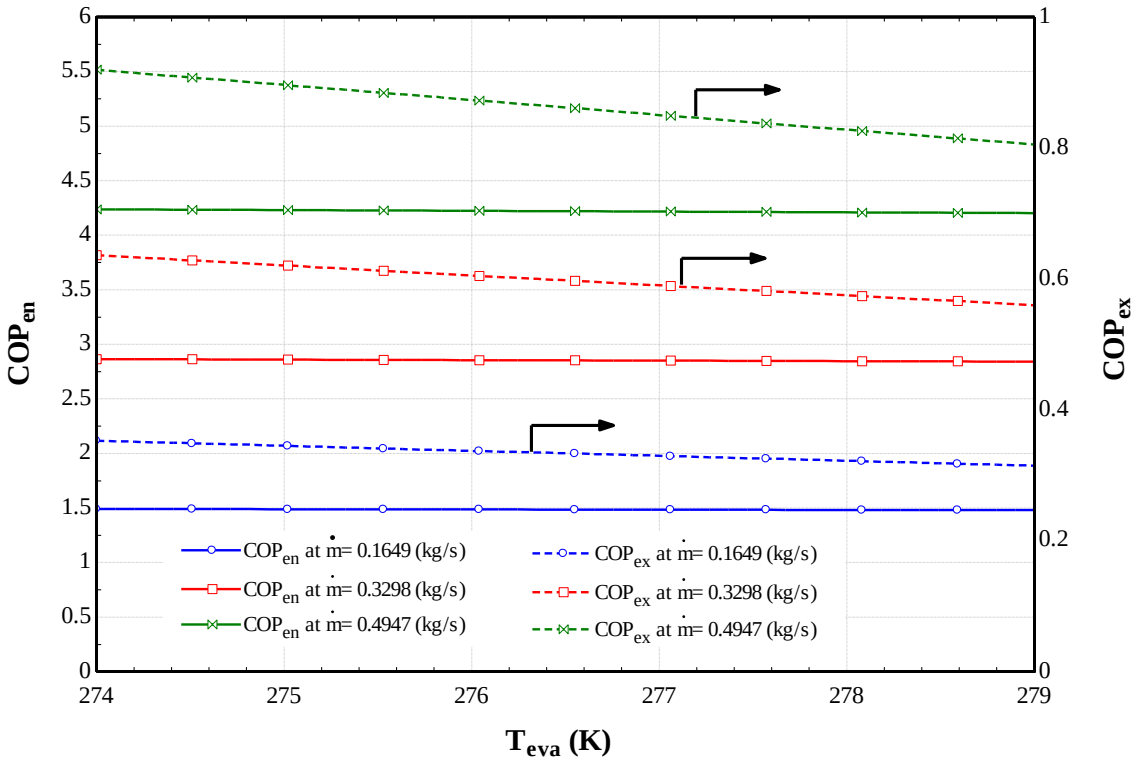

Figure 5.1: Effects of Evaporator Temperature on COP_{en} and COP_{ex}

5.2.2 Effect of Evaporator Temperature on ε_{en} and ε_{ex}

Energetic and exergetic overall utilization factors (ε_{en} and ε_{ex}) indicate the quality performance of the entire multi-generation system. By varying the evaporator temperature in TEAS from 274K to 279K, ε_{en} will decrease slightly for three amounts of TEAS mass flow (0.1649, 0.3298 and 0.4947 kg/s), from 2.475 to 2.464, 3.848 to 3.825 and 5.222 to 5.187, respectively. Likewise, there is the same trend for ε_{ex} with the difference that the slope is not as much of ε_{en}. By increasing evaporator temperature from 274K to 279K, ε_{en} will increase for the same amounts of mass flow, from 1.135 to 1.097, 1.418 to 1.342 and 1.702 to 1.587, respectively. In is noticeable that by increasing the mass flow, overall utilization factor will increase (Figure 5.2).

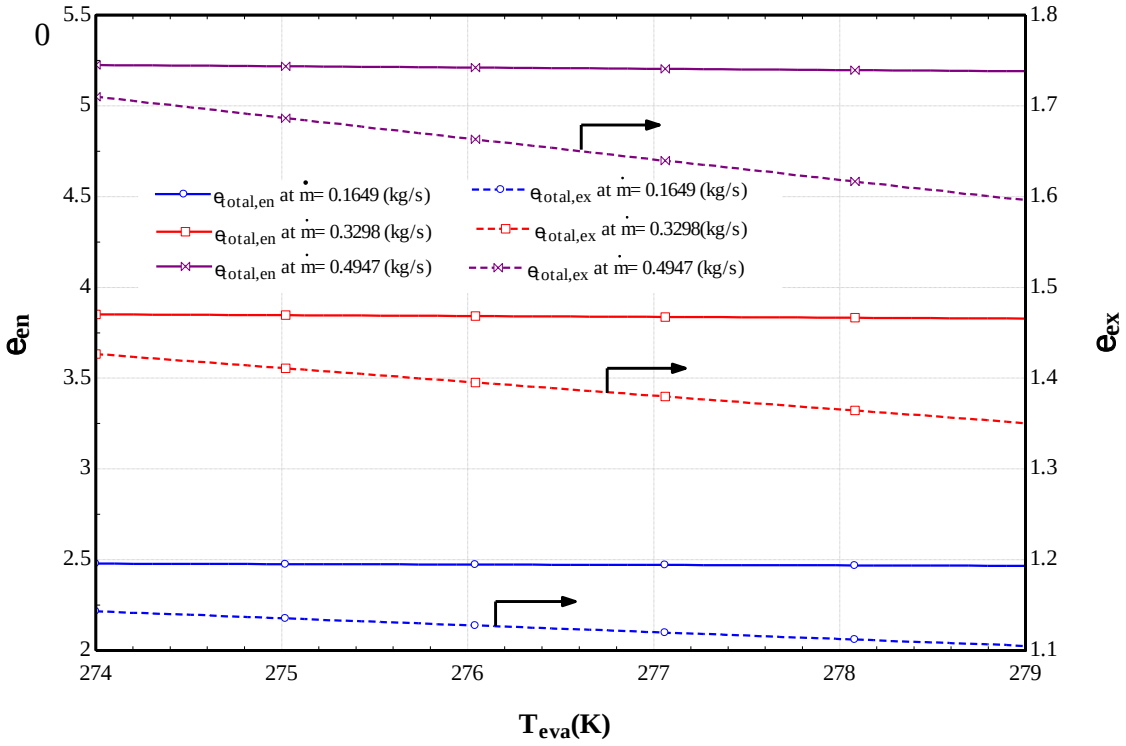

Figure 5.2: Effect of Evaporator Temperature on Overall Utilization Factor

5.2.3 The Effect of Evaporator Temperature on Cooling Load and the Rate of Condensed Water in an Air-Conditioning System

As shown in Figure 5.3, by increasing the evaporator temperature from 274K to 279K, the difference between evaporator temperature and environment temperature will decrease, and therefore, the produced cooling load will reduce from 413.18kW to 410.4kW. Also, by increasing the evaporator temperature, the rate of condensed water in the air-conditioning system will increase. Considering the energy balance equation for the air-conditioning system as a control volume, it is obvious that a decrease in the cooling load will lead to an increase in condensed water volume (from 0.9325kg/s to 0.9909kg/s for the proposed system).

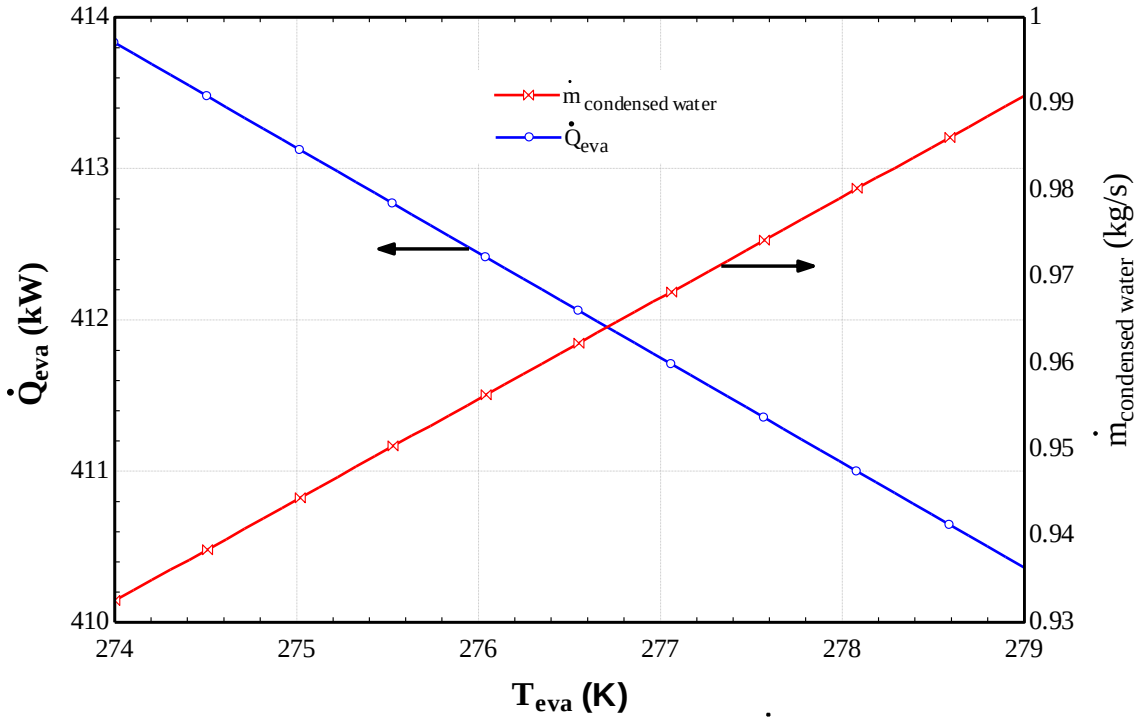

Figure 5.3: Effect of Evaporator Temperature on $\dot{Q}_{eva}$ and $\dot{m}_{condensedwater}$

5.2.4 Effect of Specific Humidity on Air-conditioning System

Henceforth, the effect of varying specific humidity (RH) on the air-conditioning system is discussed. As shown in the results, by increasing the RH from 0.4 to 0.7 the air-conditioning system efficiency will increase from 22% to 31%, 43% to 56% and 61% to 79% for the three amounts of mass flow rate (2, 4 and 6 kg/s), respectively. Figure 5.4 shows that the air-conditioning system efficiency will increase in higher specific humidity, which means the amount of water condensed from the air will increase in higher humidity.

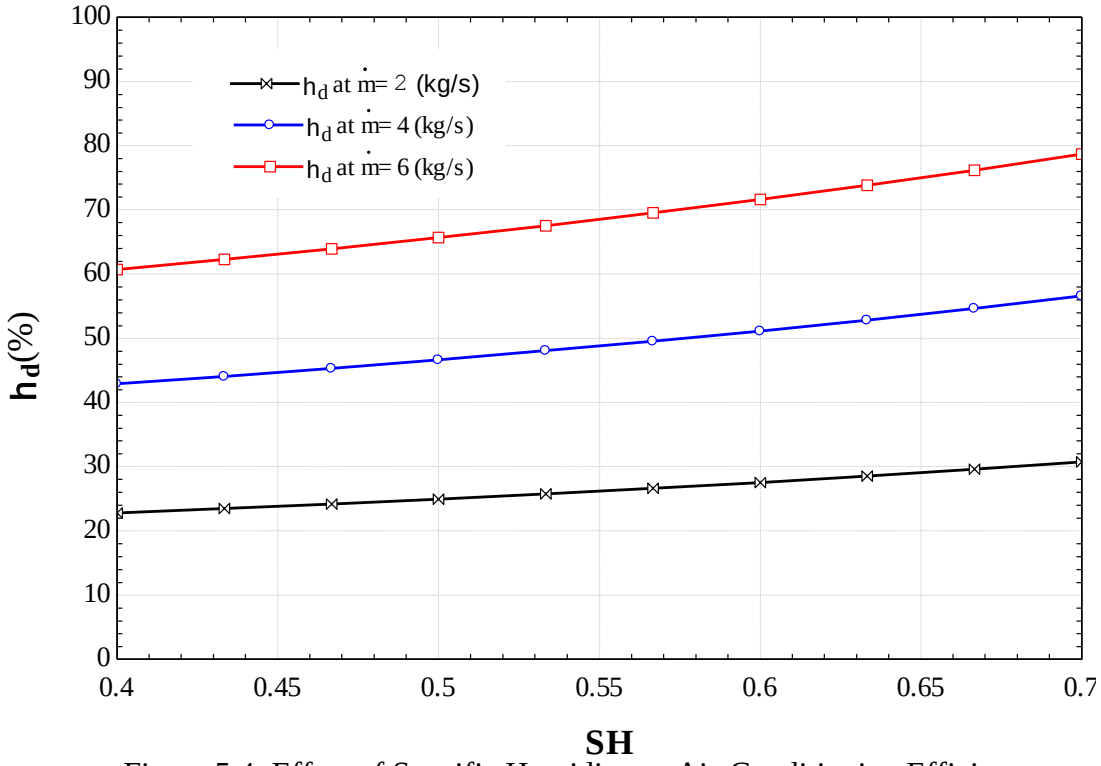

Figure 5.4: Effect of Specific Humidity on Air-Conditioning Efficiency

5.2.5 Effect of Specific Humidity on Energetic and Exergetic Utilization Factor

An increase in specific Humidity as a crucial parameter has an adverse impact on exergetic utilization factor (Figure 5.5). However, increasing specific humidity does not have any effect on energetic utilization factor. The reason is that in energetic analysis, irreversibility and loss do not come into account; therefore, energetic utilization factor will be constant numbers of 3.21 and 2.464 for both air velocities to the air-conditioning system (10m/s and 5m/s). In addition, by increasing specific humidity from 0.4 to 0.7, exergetic utilization factor will decrease from 1.08 to 1.052 and from 1.166 to 1.111 for different air velocities of 5m/s and 10m/s, respectively. As a result, it is desirable that the system work with a higher air velocity and a less specific humidity of environmental air.

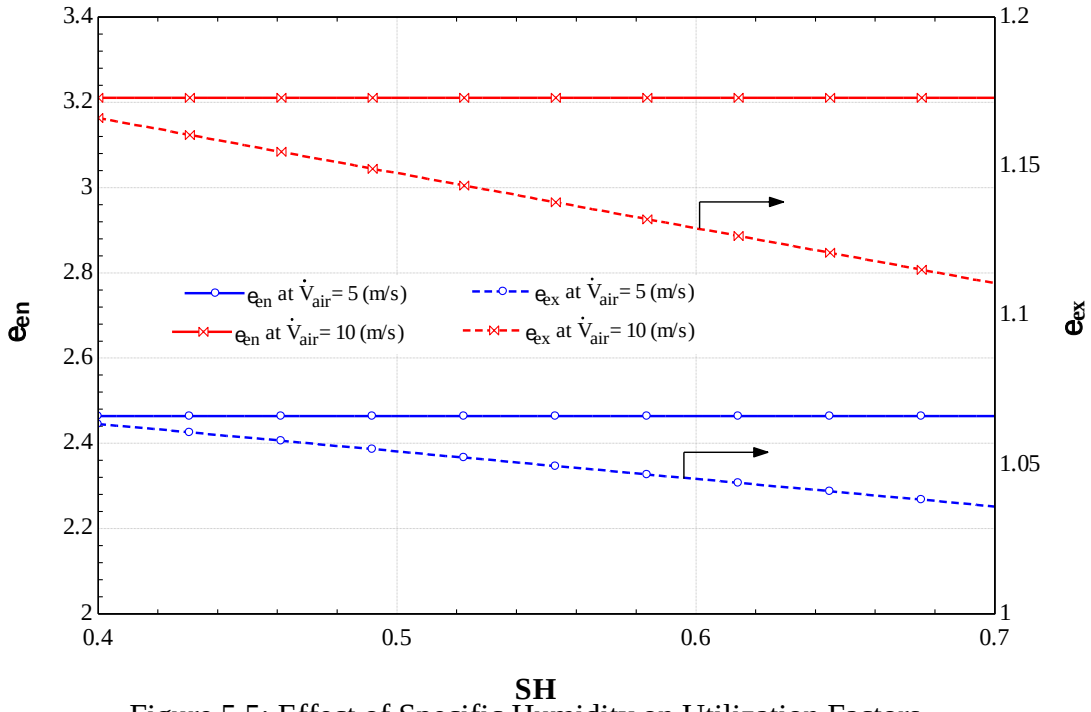

Figure 5.5: Effect of Specific Humidity on Utilization Factors

5.2.6 Effect of Geothermal Water Temperature

As shown in Figure 5.6, by raising the geothermal water temperature from 400K to 500K, both ε_{en} and ε_{ex} will increase from 2.354 to 2.467 and 1.055 to 1.105, respectively. By increasing geothermal temperature, the amount of heat, which is injected into the system, will lead to an increase in all the relative parameters such as TEAS COPs, heat rate of the boiler in ORC and the hot water supply for the buildings that means the increase can affect the whole system.

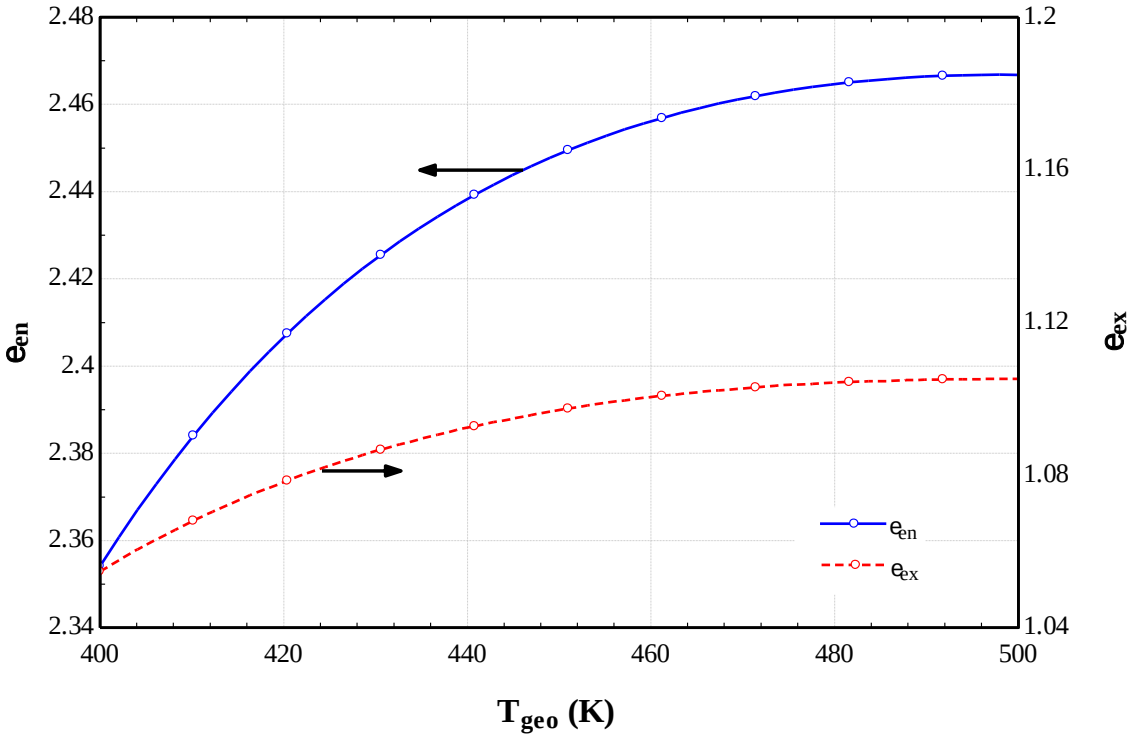

Figure 5.6: Effect of Geothermal Water Temperature on $\mathcal{E}_{en}$ and $\mathcal{E}_{ex}$

5.2.7 Effect of Inlet Geothermal Water Temperature on Total Produced Power and Heat Rate of High Temperature Generator

It is natural that by enhancing the geothermal water temperature, the heat rate of high temperature generator (HTG) will increase because of the high temperature inlet water (with the same mass flow rate). The analysis shows that by increasing the geothermal temperature from 450K to 500K, the heat rate of HTG will increase from 195.1kW to 293.4kW. Moreover, as shown in Figure 5.7, geothermal temperature growth has a positive effect on the total power produced by ORC. By increasing the geothermal temperature, the amount of total power will increase from 303.6kW to 138.7kW because of the extra heat that is absorbed by the boiler.

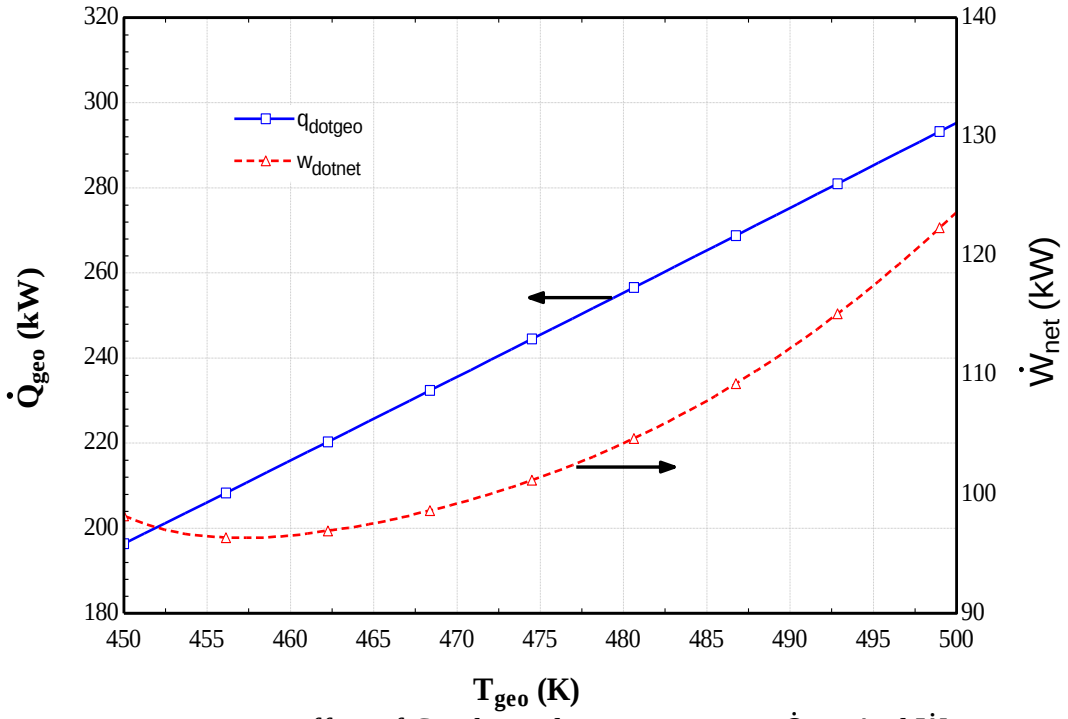

Figure 5.7: Effect of Geothermal Temperature on $\dot{Q}_{geo}$ And $\dot{W}_{net}$

5.2.8 Effect of Geothermal Temperature on $\dot{V}_{H_2}$ and $\dot{Q}_{HW}$

Since a rise in the geothermal inlet water temperature makes the produced power by ORC to grow, the amount of power that feeds the electrolyzer to produce the hydrogen will also increase. As illustrated in figure 5.8, increasing geothermal temperature from 475K to 500k, leads to an increase in the volume rate of hydrogen from 0.004873 to 0.005944L/s. Apart from that, the heat rate of hot water will also increase from 8.365kW to 112.9kW because of the high geothermal temperature left in the boiler.

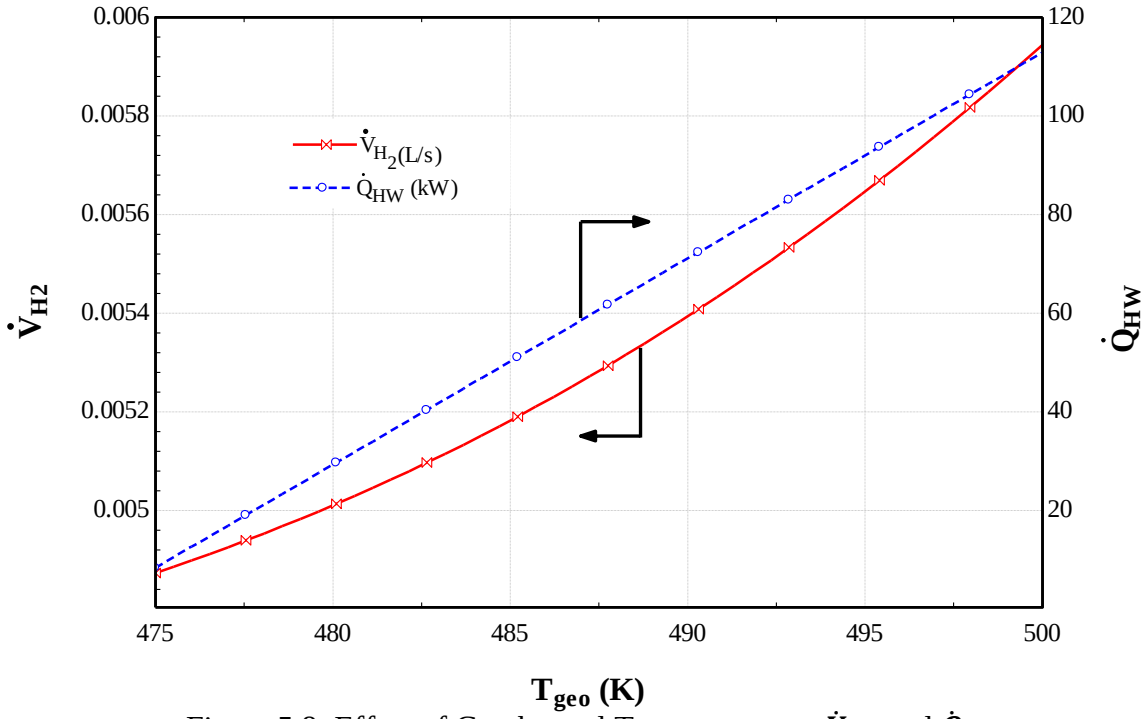

Figure 5.8: Effect of Geothermal Temperature on $\dot{V}_{H_2}$ and $\dot{Q}_{HW}$

5.2.9 Effect of Ambient (Environment) Temperature on COP_{en} and COP_{ex}

As shown in figure 5.9, by changing the ambient temperature, there is a distinct variation in COP_{en} since the energetic coefficient of performance does no account for the losses from the system. That is why COP_{en} will be the same during these conditions and just by increasing the mass flow for the amounts of 1, 2 and 3kg/s, COP_{en} will decrease as 1.479, 0.7397 and 0.4931, respectively. By increasing the ambient temperature, COP_{ex} will increase because of the less difference between the system and the ambient temperature. Consequently, if the ambient temperature rises from 295 to 320K, COP_{ex} will increase respectively from 0.2725 to 0.6733, 0.1362 to 0.3367 and 0.09083 to 0.2244 for 1, 2 and 3kg/s of mass flow in absorption system.

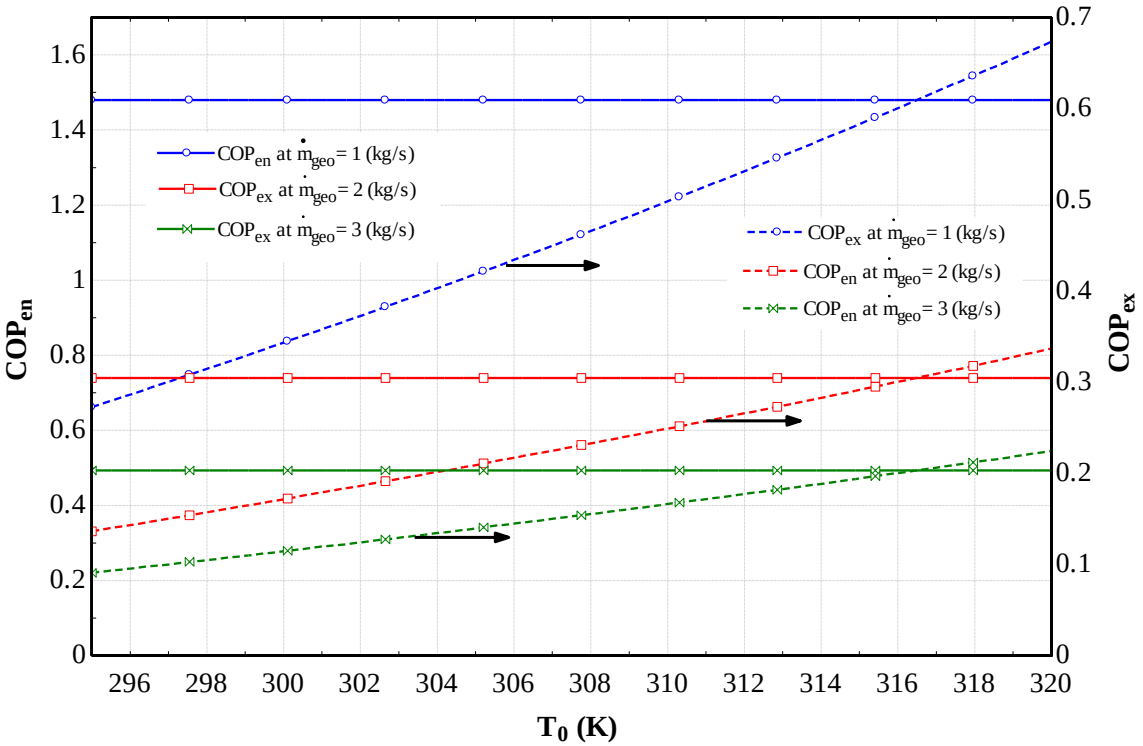

Figure 5.9: Effects of Ambient Temperature on COP_{en} and COP_{ex}

5.2.10 Effect of Ambient Temperature on $\mathcal{E}_{en}$ and $\mathcal{E}_{ex}$

Increasing the ambient temperature has the same effect on utilization factors such as COPs. As shown in Figure 5.10, when the ambient temperature increases from 290K to 320k, $\mathcal{E}_{en}$ will remain constant as 2.464, 1.232 and 0.821 for varying the geothermal mass flow of 1, 2 and 3kg/s. In exergetic analysis when the ambient temperature increases with the varying geothermal mass flow of 1, 2 and 3kg/s, $\mathcal{E}_{ex}$ changes from 1.081 to 1.228, 0.5403 to 0.6136 and 0.36 to 0.4089, correspondingly. The rise in ambient temperature forces ambient enthalpy and entropy to increase as well. This will cause a bigger difference between the system and ambient exergy that will cause the exergetic utilization factor to increase.

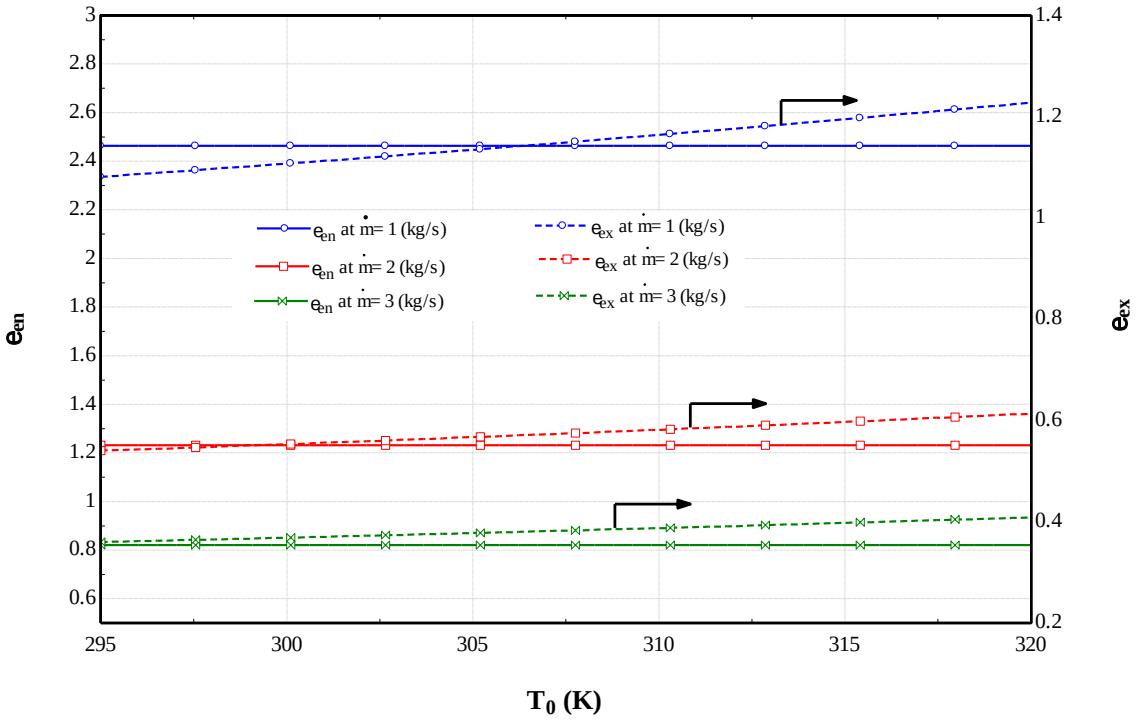

Figure 5.10: Effect of Ambient Temperature on $\mathcal{E}_{en}$ and $\mathcal{E}_{ex}$

5.2.11 Effects of Variation in Evaporator Temperature on Exergoenvironmental Impact Factor

The exergoenvironmental impact factor refers to the effects of the integrated system on the surrounding environment. By considering this parameter, it is expected to decrease the irreversibilities in the system in order to reduce the environmental impacts. The base amount of this parameter is “zero” which shows there is no irreversibility in the system. As it is shown in the Figure 5.11, the exergoenvironmental impact factor is decreased so slightly by increasing the evaporator temperature for the three varying ambient temperature of 303K, 308K and 313K, from 0.03116 to 0.03115, 0.0315 to 0.0315 and 0.03189 to 0.03189, respectively. Figure 5.10 can be justified by considering the point that in higher ambient temperature, the exergy destruction rate is decreased and by increasing the evaporator temperature from 274K to 279K the exergoenvironmental impact factor is reduced because of lower exergy destruction in higher evaporator temperature.

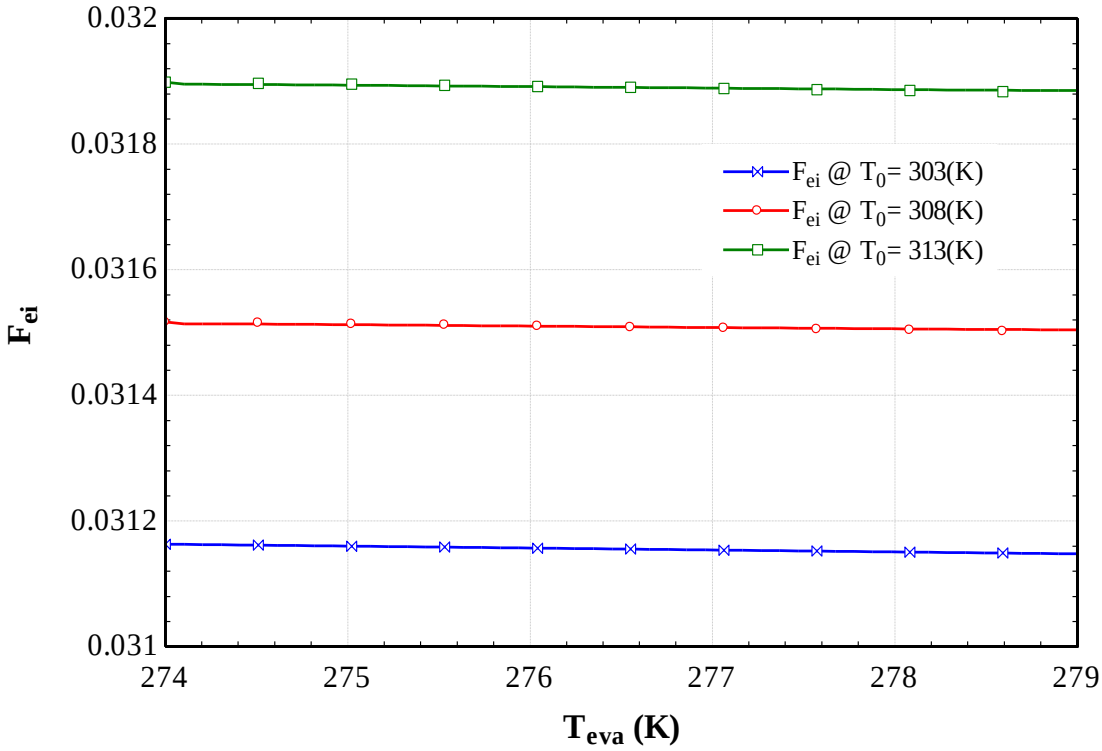

Figure 5.11: Effects of Variation in Evaporator Temperature on Exergoenvironmental Impact Factor

5.2.12 Effects of Variation in Evaporator Temperature Effect on Exergoenvironmental Impact Coefficient

The exergoenvironmental impact coefficient is the parameter that is directly come from exergy effinecy of the system. As an ideal case, it is expected that exergoenvironmental impact coefficient is reached to 13 that showes that the system has no exergy destruction. In this system designing, By varying evaporator temperature from 274K to 279K, there is an upward trend of C_{ei} for three different ambient tepmerature of 303K, 308K and 313K. The simulation shows that bay increasing the evaporator temperature this parameter is increased from 0.8592 to 0.8592, 0.837 to 0.837 and 0.8145 to 0.8145, respectively. It is crystal clear that in the cooler environment, system works better (lower exergy destruction), so by considering lower ambient temperature and higher evaporator temperature system

works with lower exergy destruction and higher exergoenvironmental impact coefficient (near to 1).

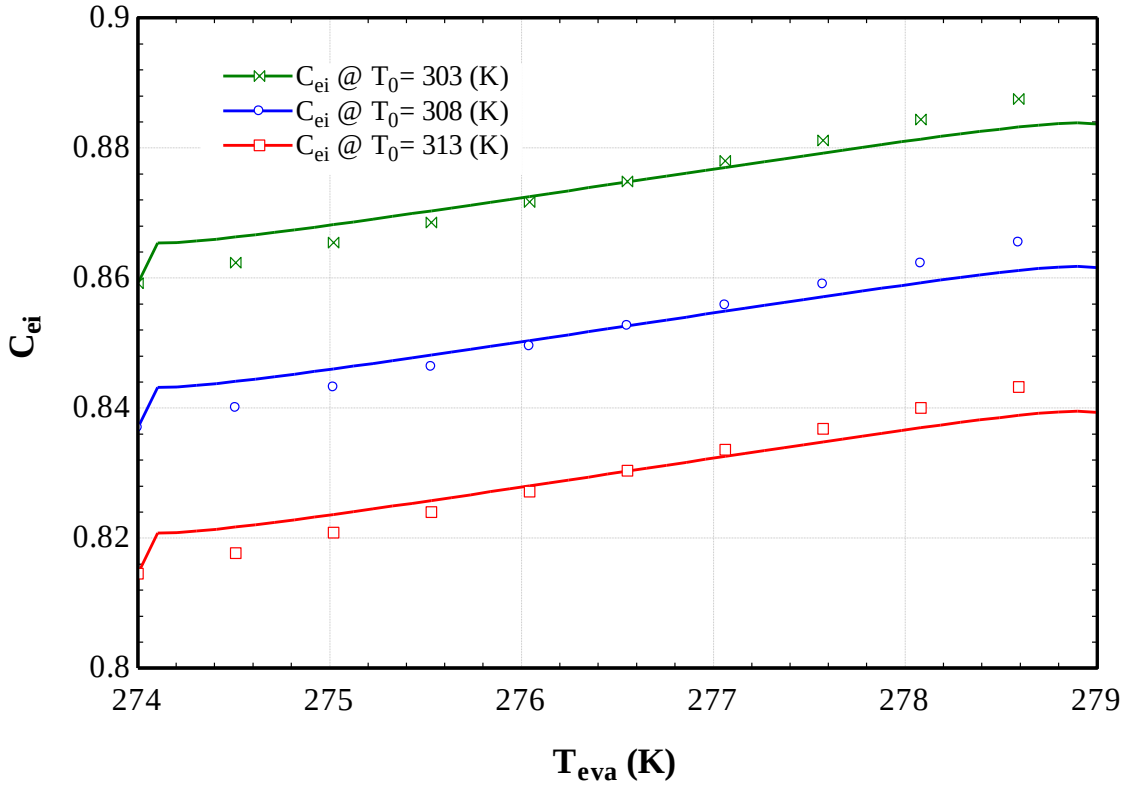

Figure 5.12: Effects of Variation in Evaporator Temperature Effect on Exergoenvironmental Impact Coefficient

5.2.13 Effects of Variation in Evaporator Temperature on Exergoenvironmental Impact Index

The exergoenvironmental impact index is a vital factor to investigate whether the system has any negative impacts on the environment due to the exergy destruction or waste exergy or not. It is desired that the value of Exergoenvironmental impact index be as small as possible. The exergoenvironmental impact index is calculated by multiplying exergoenvironmental impact factor with exergoenvironmental impact coefficient. As it is shown in Figure 5.13, by varying the evaporator temperature from 274K to 279K for three different ambient temperatuer, all the θ_{ei} for all systems

will increase from 0.02678 to 0.02772, 0.02638 to 0.02735 and 0.02598 to 0.02697, respectively.

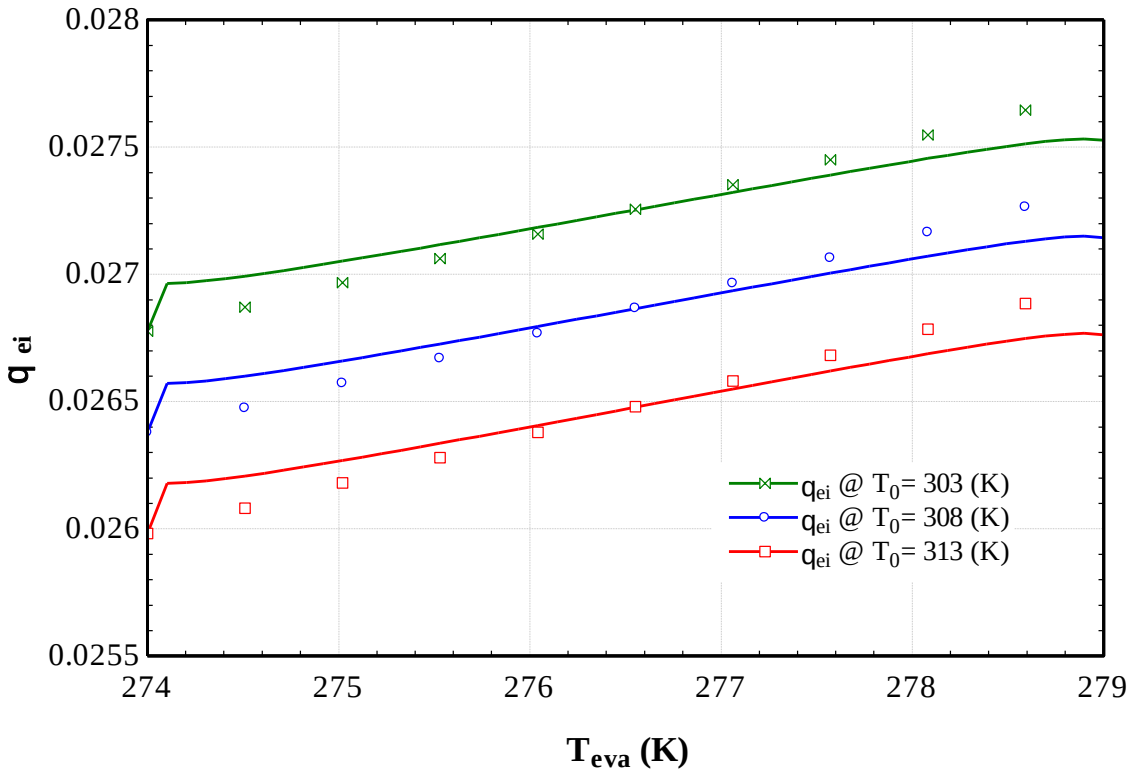

Figure 5.13: Effects of Variation in Evaporator Temperature on Exergoenvironmental Impact Index

5.2.14 Effects of Variation in Evaporator Temperature on Exergoenvironmental Impact Improvement

The exergoenvironmental impact improvement is used to investigate the environment suistability of the system. To improve the environmental suitability of the system, its exergoenvironmental impact index should be minimized. As it is shown in Figure 5.14, by varying the evaporator temperature from 274K to 279K, there is a downward trend for the $\theta_{eii.}$ By changing the ambient temperature (303K, 308K and 313K), the exergoenvironmental impact improvement is decreased from 37.35 to 36.07, 37.91 to 36.57 and 38.49 to 37.08, respectively.

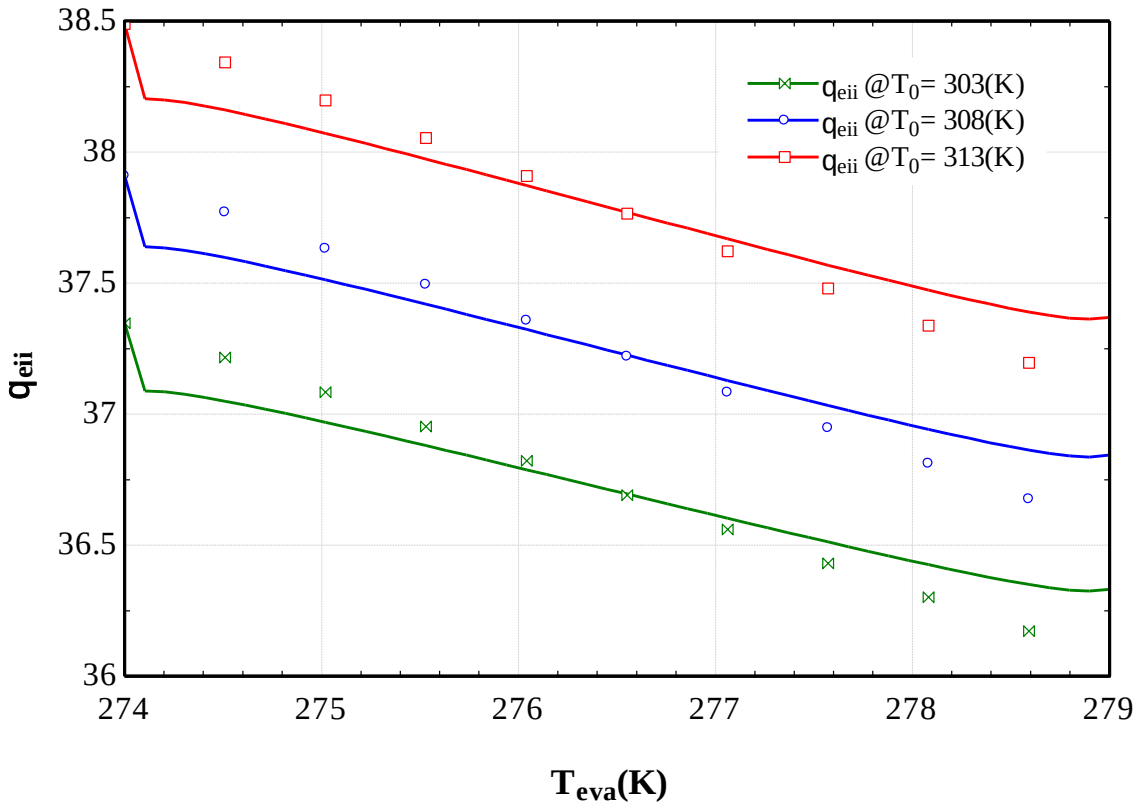

Figure 5.14: Effects of Variation in Evaporator Temperature on Exergoenvironmental Impact Improvement

5.2.15 Effects of Variation in Evaporator Temperature on Exergetic Stability Factor

The exergetic stability factor as shown in Figure 5.15 is a function of the desired output exergy, total exergy destruction, and exergy carried by the unused fuel. It is desired to obtain the value of this factor as close to "one" as possible which is logical. As it is shown in Figure 5.14, by varying the evaporator temperature from 274K to 279K for three different ambient temperatuer, all the θ_{ei} are increased.

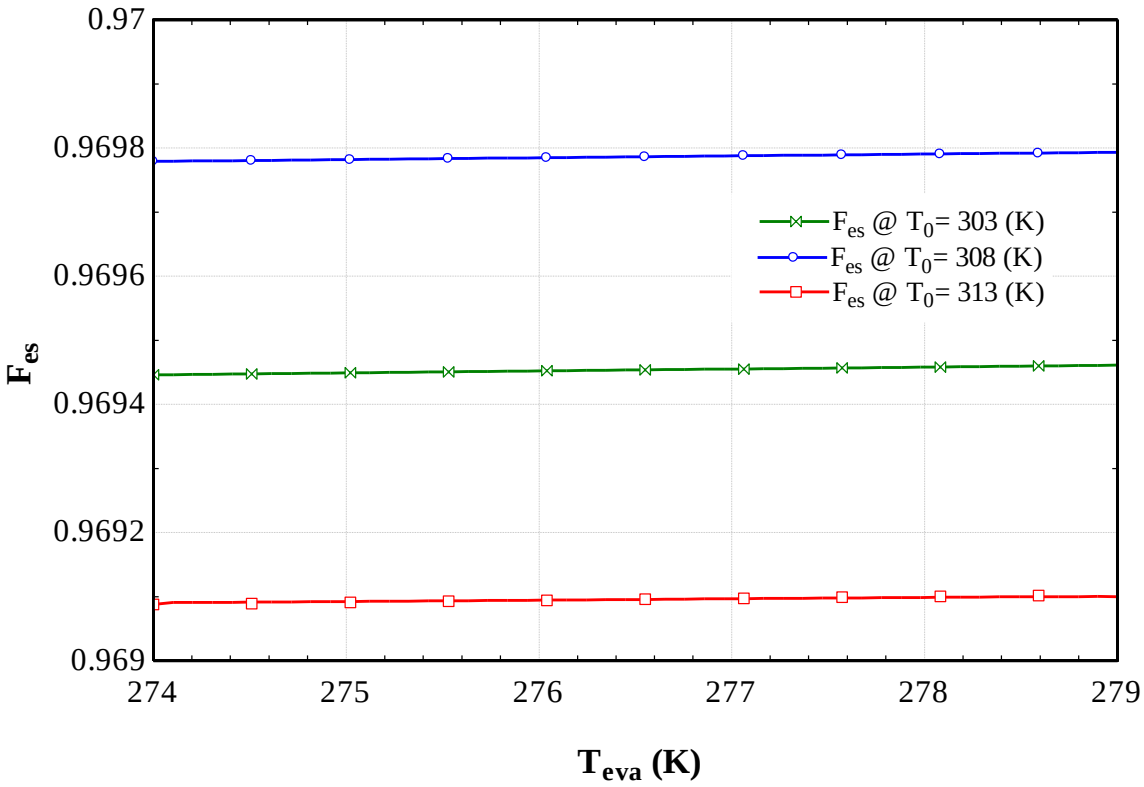

Figure 5.15: Effects of Variation in Evaporator Temperature on Exergetic Stability Factor

5.2.16 Effects of Variation in Evaporator Temperature on the Exergetic Sustainability Index

The exergetic sustainability index as shown in Figure 5.16 is the multiplication of exergetic stability factor and Exergoenvironmental impact improvement of the system. It is desired to obtain the highest possible value of exergetic sustainability index. For this evaluation, it is increased by varying the evaporator temperature from 274K to 279K in three different ambient temperatures. The results show that the exergetic sustainability index is varied from 37.3 to 35.94, 36.75 to 35.45 and 36.22 to 34.98.

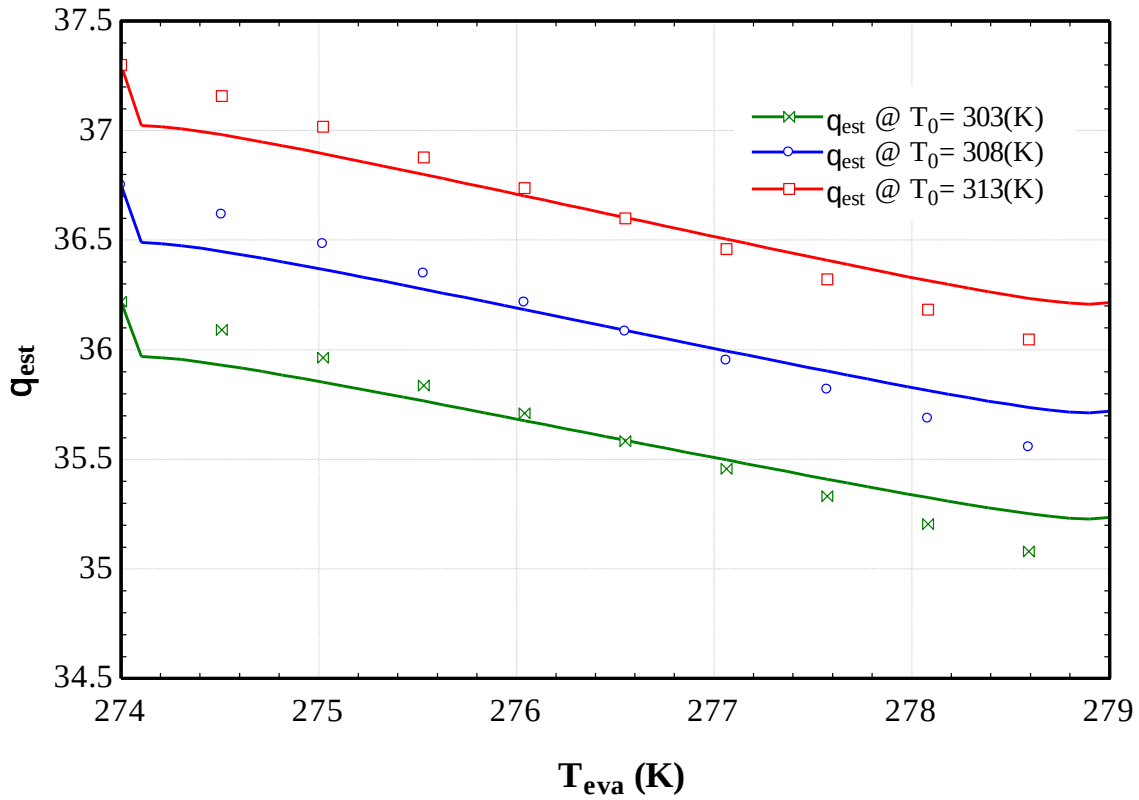

Figure 5.17: Effects of Variation in Evaporator Temperature on the Exergetic Sustainability Index

Chapter 6

CONCLUSION AND RECOMMENDATION

In the current research, a multi-generation cycle was designed including: (a) a parallel triple effect LiBr/water absorption system (parallel systems are including three separate condenser connected to the generators.), (b) an organic Rankine cycle working with ammonia, (c) an electrolyzer to produce hydrogen, (d) and an air-conditioning system based on dehumidification with a cooling process. In the proposed system, it was sought out to produce six outputs containing hydrogen from electrolyzer, power and hot water from organic cycle and cooling, heating and dry air from triple-effect absorption system. Calculating the amounts of output depending on the inlet parameter (geothermal hot water), $\mathcal{E}_{en}$ and $\mathcal{E}_{ex}$ were conducted 2.464 and 1.097, respectively. Then, a parametric study was done to investigate the effect of varying parameters. By varying the evaporator temperature from 274K to 279K, COP_{en} decreased from 1.491 to 1.479, 2.864 to 2.841 and 4.237 to 4.203 for the varying mass flows. COP_{ex} had also a significant decline from 0.3525 to 0.3145, 0.6359 to 0.5598 and 0.9194 to 0.8052 for the same mass flows (0.1649, 0.3298 and 0.4947 kg/s). Also, by increasing the evaporator temperature for the basic geothermal mass flow rate (1kg/s) $\mathcal{E}_{en}$ and $\mathcal{E}_{ex}$ decreased from 2.475 to 2.464 and 1.135 to 1.097, respectively. Moreover, an increase in the evaporator temperature caused a reduction in the cooling load from 413.18kW to 410.4kW and raised in the condensed water of the air-conditioning system from 0.9325kg/s to 0.9909kg/s. By increasing the geothermal temperature from 400 to 500K, $\mathcal{E}_{en}$ and $\mathcal{E}_{ex}$ increased respectively from

2.354 to 2.467 and 1.055 to 1.105, for the basic geothermal mass flow rate (1kg/s) and the same varying geothermal mass flow(1 to 3kg/s). By varying the geothermal water temperature from 450K to 500K, the heat rate of high temperature generator increased from 196.3kW to 295.3 kW. Also, this increase caused the total power produced by ORC to increase from 98.17 kW to 138.7 kW. It also led to the growth of hot water heat rate from 8.365kW to 112.9kW, and hydrogen production from 0.004873L/s to 0.005944L/s.

Specific humidity is a crucial parameter that affects the air-conditioning system efficiency. By increasing the specific humidity from 0.4 to 0.7, efficiency increased from 22.3% to 30.5% while $\mathcal{E}_{en}$ remained constant, and $\mathcal{E}_{ex}$ decreased. Also, the effect of ambient temperature on the COP_{en} and COP_{ex} of the absorption system was analyzed. Results showed that by increasing the ambient temperature from 295 to 320K, COP_{en} remained constant for the absorption system, and it was only decreased (1.479, 0.7397 and 0.4931) when changing the mass flow. Whereas by increasing the ambient temperature, COP_{ex} increased from 0.2725 to 0.6733, 0.1362 to 0.3367 and 0.09083 to 0.2244, respectively. Moreover, by increasing the ambient temperature, $\mathcal{E}_{en}$ remained constant for COP_{en} despite the fact that $\mathcal{E}_{ex}$ increased. Mass flow for absorption system was varied from 1 to 3kg/s of mass flow in absorption system, respectively. In addition, an inclusive simulation study has been done to analyze the effect of varying evaporator temperature on the exergoenvironmental parameters to evaluate their environmental impacts. Furthermore, by varying the evaporator temperature from 274K to 279K the environmental parameters such as exergoenvironmental impact factor, exergoenvironmental impact coefficient, exergoenvironmental impact index, exergoenvironmental impact improvement, exergetic stability factor and exergetic sustainability index will vary depending on

their characteristics but the shining point is that system will work more eco-friendly in lower evaporator temperature. The most vital parameter to examine systems in the aspect of environmental is to evaluate their irreversibility (exergy destruction) or in another hand their losses to the environment. Therefore, by implementing the multi-generation cycle, a higher COP_{en} and COP_{ex} can be reached, and the six outputs can be supplied to the demand side to keep the environmental concerns in parallel.

REFERENCES

[1] Ozgur Colpan, C., Dincer, I., & Hamdullahpur, F. (2009). The reduction of greenhouse gas emissions using various thermal systems in a landfill site. *International Journal of Global Warming*, *1*(1-3), 89-105.

[2] Spahni, R., Chappellaz, J., Stocker, T. F., Loulergue, L., Hausammann, G., Kawamura, K., ... & Jouzel, J. (2005). Atmospheric methane and nitrous oxide of the late Pleistocene from Antarctic ice cores. *Science*, *310*(5752), 1317-1321.

[3] Ratlamwala, T. A. H., El-Sinawi, A. H., Gadalla, M. A., & Aidan, A. (2012). Performance analysis of a new designed PEM fuel cell. *International Journal of Energy Research*, *36*(11), 1121-1132.

[4] Ahmadi, P., & Dincer, I. (2010). Exergoenvironmental analysis and optimization of a cogeneration plant system using Multimodal Genetic Algorithm (MGA). *Energy*, *35*(12), 5161-5172.

[5] Al-Sulaiman, F. A., Dincer, I., & Hamdullahpur, F. (2010). Exergy analysis of an integrated solid oxide fuel cell and organic Rankine cycle for cooling, heating and power production. *Journal of power sources*, *195*(8), 2346-2354.

[6] Ahmadi, P., Rosen, M. A., & Dincer, I. (2011). Greenhouse gas emission and exergo-environmental analyses of a trigeneration energy system. *International Journal of Greenhouse Gas Control*, *5*(6), 1540-1549.

[7] Dincer, I., & Zamfirescu, C. (2012). Renewable-energy-based multigeneration systems. *International Journal of Energy Research*, *36*(15), 1403-1415.

[8] Ahmadi, P., Rosen, M. A., & Dincer, I. (2012). Multi-objective exergy-based optimization of a polygeneration energy system using an evolutionary algorithm. *Energy*, *46*(1), 21-31.

[9] Khaliq, A., Kumar, R., & Dincer, I. (2009). Performance analysis of an industrial waste heat-based trigeneration system. *International journal of energy research*, *33*(8), 737-744.

[10] Ratlamwala, T. A. H., & Dincer, I. (2013). Development of a geothermal based integrated system for building multigenerational needs. *Energy and Buildings*, *62*, 496-506.

[11] Kanoglu, M., & Bolatturk, A. (2008). Performance and parametric investigation of a binary geothermal power plant by exergy. *Renewable Energy*, *33*(11), 2366-2374.

[12] Dincer, I., & Ratlamwala, T. A. H. (2013). Development of novel renewable energy based hydrogen production systems: a comparative study. *Energy Conversion and Management*, *72*, 77-87.

[13] Zaigham, N. A., Nayyar, Z. A., & Hisamuddin, N. (2009). Review of geothermal energy resources in Pakistan. *Renewable and Sustainable Energy Reviews*, *13*(1), 223-232.

[14] Kilkis, B. (2011). A lignite–geothermal hybrid power and hydrogen production plant for green cities and sustainable buildings. *International Journal of Energy Research*, *35*(2), 138-145.

[15] Ghafghazi, S., Sowlati, T., Sokhansanj, S., & Melin, S. (2010). Techno-economic analysis of renewable energy source options for a district heating project. *International Jo*

[16] Balli, O., Aras, H., & Hepbasli, A. (2007). Exergetic performance evaluation of a combined heat and power (CHP) system in Turkey. *International Journal of Energy Research*, *31*(9), 849-866.

[17] Balli, O., Aras, H., & Hepbasli, A. (2008). Exergoeconomic analysis of a combined heat and power (CHP) system. *International Journal of Energy Research*, *32*(4), 273-289.

[18] Gunerhan, G. G., Kocar, G., & Hepbasli, A. (2001). Geothermal energy utilization in Turkey. *International Journal of Energy Research*, *25*(9), 769-784.

[19] Bilgen, E. (2000). Exergetic and engineering analyses of gas turbine based cogeneration systems. *Energy*, *25*(12), 1215-1229.

[20] Huangfu, Y., Wu, J. Y., Wang, R. Z., & Xia, Z. Z. (2007). Experimental investigation of adsorption chiller for Micro-scale BCHP system application. *Energy and buildings*, *39*(2), 120-127.

[21] Mago, P. J., Hueffed, A., & Chamra, L. M. (2010). Analysis and optimization of the use of CHP–ORC systems for small commercial buildings. *Energy and Buildings*, *42*(9), 1491-1498.

[22] Bianchi, M., De Pascale, A., & Melino, F. (2013). Performance analysis of an integrated CHP system with thermal and electric energy storage for residential application. Applied Energy, 112, 928-938.

[23] Havelský, V. (1999). Energetic efficiency of cogeneration systems for combined heat, cold and power production. *International Journal of Refrigeration*, *22*(6), 479-485.

[24] Mıguez, J. L., Murillo, S., Porteiro, J., & López, L. M. (2004). Feasibility of a new domestic CHP trigeneration with heat pump: I. Design and development. *Applied thermal engineering*, *24*(10), 1409-1419.

[25] Porteiro, J., Mıguez, J. L., Murillo, S., & López, L. M. (2004). Feasibility of a new domestic CHP trigeneration with heat pump: II. Availability analysis. Applied thermal engineering, 24(10), 1421-1429.

[26] Cihan, A., Hacıhafızog˘lu, O., & Kahveci, K. (2006). Energy–exergy analysis and modernization suggestions for a combined-cycle power plant. *International Journal of Energy Research*, *30*(2), 115-126.

[27] Barelli, L., Bidini, G., Gallorini, F., & Ottaviano, A. (2011). An energetic–exergetic analysis of a residential CHP system based on PEM fuel cell. *Applied Energy*, *88*(12), 4334-4342.

[28] Bingöl, E., Kılkış, B., & Eralp, C. (2011). Exergy based performance analysis of high efficiency poly-generation systems for sustainable building applications. *Energy and Buildings*, *43*(11), 3074-3081.

[29] El-Emam, R. S., & Dincer, I. (2011). Energy and exergy analyses of a combined molten carbonate fuel cell–Gas turbine system. *international journal of hydrogen energy*, *36*(15), 8927-8935.

[30] Akkaya, A. V., Sahin, B., & Erdem, H. H. (2008). An analysis of SOFC/GT CHP system based on exergetic performance criteria. *International Journal of Hydrogen Energy*, *33*(10), 2566-2577.

[31] Al-Sulaiman, F. A., Dincer, I., & Hamdullahpur, F. (2010). Energy analysis of a trigeneration plant based on solid oxide fuel cell and organic Rankine cycle. *International Journal of Hydrogen Energy*, *35*(10), 5104-5113.

[32] Pospisil, J., Fiedler, J., Skala, Z., & Baksa, M. (2006). Comparison of cogeneration and trigeneration technology for energy supply of tertiary buildings. *WSEAS Transactions on Heat and Mass Transfer*, *1*(3), 262-267.

[33] Al-Sulaiman, F. A., Hamdullahpur, F., & Dincer, I. (2011). Performance comparison of three trigeneration systems using organic rankine cycles. *Energy*, *36*(9), 5741-5754.

[34] Martins, L. N., Fábrega, F. M., & d'Angelo, J. V. H. (2012). Thermodynamic performance investigation of a trigeneration cycle considering the influence of operational variables. *Procedia Engineering*, *42*, 1879-1888.

[35] Chicco, G., & Mancarella, P. (2005, November). Planning aspects and performance indicators for small-scale trigeneration plants. In *2005 International Conference on Future Power Systems* (pp. 6-pp). IEEE.

[36] Minciuc, E., Le Corre, O., Athanasovici, V., Tazerout, M., & Bitir, I. (2003). Thermodynamic analysis of tri-generation with absorption chilling machine. *Applied thermal engineering*, *23*(11), 1391-1405.

[37] Buck, R., & Friedmann, S. (2007). Solar-assisted small solar tower trigeneration systems. Journal of Solar Energy Engineering, 129(4), 349-354.

[38] Dincer, I., & Rosen, M. A. (2012). *Exergy: energy, environment and sustainable development*. Newnes.

[39] Khaliq, A. (2009). Exergy analysis of gas turbine trigeneration system for combined production of power heat and refrigeration. *International Journal of Refrigeration*, *32*(3), 534-545.

[40] Mago, P. J., & Hueffed, A. K. (2010). Evaluation of a turbine driven CCHP system for large office buildings under different operating strategies. *Energy and Buildings*, *42*(10), 1628-1636.

[41] Dincer, I. (2007). Environmental and sustainability aspects of hydrogen and fuel cell systems. *International Journal of Energy Research*, *31*(1), 29-55.

[42] Mago, P. J., & Smith, A. D. (2012). Evaluation of the potential emissions reductions from the use of CHP systems in different commercial buildings. *Building and Environment*, *53*, 74-82.

[43] Hosseini, M., Dincer, I., Ahmadi, P., Avval, H. B., & Ziaasharhagh, M. (2013). Thermodynamic modelling of an integrated solid oxide fuel cell and micro gas turbine system for desalination purposes. *International Journal of Energy Research*, *37*(5), 426-434.

[44] Ratlamwala, T. A. H., Gadalla, M. A., & Dincer, I. (2011). Performance assessment of an integrated PV/T and triple effect cooling system for hydrogen and cooling production. *international journal of hydrogen energy*, *36*(17), 11282-11291.

[45] Ratlamwala, T. A. H., Dincer, I., & Gadalla, M. A. (2012). Performance analysis of a novel integrated geothermal-based system for multi-generation applications. *Applied Thermal Engineering*, *40*, 71-79.

[46] Ozturk, M., & Dincer, I. (2013). Thermodynamic analysis of a solar-based multi-generation system with hydrogen production. *Applied Thermal Engineering, 51*(1), 1235-1244.

[47] Ratlamwala, T. A. H., Dincer, I., & Gadalla, M. A. (2012). Thermodynamic analysis of an integrated geothermal based quadruple effect absorption system for multigenerational purposes. *Thermochimica acta, 535,* 27-35.

APPENDIX

Appendix A: Engineering Equation Solver Software Codes

```
t[2]=303.5

t[3]=313

t[4]=325

t[5]=315

s[2]=s_LiBrH2O(T[2],x[2])

s[3]=s_LiBrH2O(T[3],x[3])

s[4]=s_LiBrH2O(T[4],x[4])

s[5]=s_LiBrH2O(T[5],x[5])

m_dot[2]=1

m_dot[3]=1

m_dot[4]=0.8351

m_dot[5]=0.8351

h[3]=h_LiBrH2O(T[3],x[3])

p[2]=1.8

h[2]=h_LiBrH2O(T[2],x[2])

h[5]=h_LiBrH2O(T[5],x[5])

h[4]=h_LiBrH2O(T[4],x[4])

x[3]=x_LiBrH2O(T[3],P[3])

p[3]=1.8

p[4]=1.8

p[5]=1.8

x[2]=x_LiBrH2O(T[2],P[2])

x[5]=x_LiBrH2O(T[5],P[5])
```

x[4]=x_LiBrH2O(T[4],P[4])

q_dotLHE=+m_dot[4]*h[4]-m_dot[5]*h[5]

ex[2]=m_dot[2]*((h[2]-h[0])-t[0]*(s[2]-s[0]))

ex[3]=m_dot[3]*((h[3]-h[0])-t[0]*(s[3]-s[0]))

ex[4]=m_dot[4]*((h[4]-h[0])-t[0]*(s[4]-s[0]))

ex[5]=m_dot[5]*((h[5]-h[0])-t[0]*(s[5]-s[0]))

exqLHE=(1-t[0]/(t[4]/4+t[2]/4+t[3]/4+t[5]/4))* q_dotLHE

exdLHE=ex[2]+ex[4]+exqLHE-ex[3]-ex[5]

"for LTG"

t[20]=358

t[7]=348

m_dot[20]=0.8641

m_dot[7]=0.0289

h[20]=h_LiBrH2O(T[20],x[20])

h[7]=Enthalpy(Water,T=T[7],P=P[7])

s[7]=Entropy(Water,T=T[7],P=P[7])

s[20]=s_LiBrH2O(T[20],x[20])

x[20]=x_LiBrH2O(T[20],P[20])

p[20]=1.8

p[7]=1.8

q_dotLTG=-m_dot[4]*h[4]-m_dot[7]*h[7]+m_dot[20]*h[20]

ex[7]=m_dot[7]*((h[7]-h[0])-t[0]*(s[7]-s[0]))

ex[20]=m_dot[20]*((h[20]-h[0])-t[0]*(s[20]-s[0]))

exqLTG=(1-t[0]/(t[20]/3+t[4]/3+t[7]/3)) *q_dotLTG

exdLTG=ex[20]-ex[4]+exqLTG-ex[7]

"w_dotpump1=m_dot[1]*(p[2]-p[1])/0.85"

R[1]=rho_LiBrH2O(T[1],X[1])

v[1]=1/R[1]

w_dotpump1=(m_dot[1]*(v[1]*(p[2]-p[1])))/0.85

R[3]=rho_LiBrH2O(T[3],X[3])

v[3]=1/R[3]

w_dotpump2=(m_dot[3]*(v[3]*(p[12]-p[3])))/0.85

R[12]=rho_LiBrH2O(T[12],X[12])

v[12]=1/R[12]

w_dotpump3=(m_dot[12]*(v[12]*(p[14]-p[12])))/0.85

"for MHE"

t[12]=393

t[18]=410

t[19]=380

m_dot[18]=0.8641

m_dot[12]=1

m_dot[19]=0.8641

h[18]=h_LiBrH2O(T[18],x[18])

h[12]=h_LiBrH2O(T[12],x[12])

h[19]=h_LiBrH2O(T[19],x[19])

s[12]=s_LiBrH2O(T[12],x[12])

s[18]=s_LiBrH2O(T[18],x[18])

s[19]=s_LiBrH2O(T[19],x[19])

p[19]=4.5

p[18]=4.5

p[12]=4.5

x[18]=x_LiBrH2O(T[18],P[18])

x[12]=x_LiBrH2O(T[12],P[12])

x[19]=x_LiBrH2O(T[19],P[19])

q_dotMHE=m_dot[19]*h[19]-m_dot[18]*h[18]

ex[12]=m_dot[12]*((h[12]-h[0])-t[0]*(s[12]-s[0]))

ex[18]=m_dot[18]*((h[18]-h[0])-t[0]*(s[18]-s[0]))

ex[19]=m_dot[19]*((h[19]-h[0])-t[0]*(s[19]-s[0]))

exqMHE=(1-t[0]/(t[18]/4+t[3]/4+t[12]/4+t[19]/4)) *q_dotMHE

exdMHE=-ex[3]-ex[18]-exqMHE+ex[12]+ex[19]

"for MTG"

t[17]=420

t[24]=412

m_dot[17]=0.912

m_dot[24]=0.0479

h[17]=h_LiBrH2O(T[17],x[17])

h[24]=Enthalpy(Water,T=T[24],P=P[24])

s[17]=s_LiBrH2O(T[17],x[17])

s[24]=Entropy(Water,T=T[24],P=P[24])

p[24]=4.5

x[17]=x_LiBrH2O(T[17],P[17])

p[17]=4.5

q_dotMTG=m_dot[24]*h[24]+m_dot[18]*h[18]-m_dot[17]*h[17]

ex[17]=m_dot[17]*((h[17]-h[0])-t[0]*(s[17]-s[0]))

ex[24]=m_dot[24]*((h[24]-h[0])-t[0]*(s[24]-s[0]))

exqMTG=(1-t[0]/(t[17]/3+t[24]/3+t[18]/3)) *q_dotMTG

exdMTG=ex[17]+exqMTG-ex[24]-ex[18]

"for HHe"

t[14]=460

t[15]=473

t[16]=433

m_dot[14]=1

m_dot[15]=0.912

m_dot[16]=0.912

h[14]=h_LiBrH2O(T[14],x[14])

h[15]=h_LiBrH2O(T[15],x[15])

h[16]=h_LiBrH2O(T[16],x[16])

s[14]=s_LiBrH2O(T[14],x[14])

s[15]=s_LiBrH2O(T[15],x[15])

s[16]=s_LiBrH2O(T[16],x[16])

x[14]=x_LiBrH2O(T[14],P[14])

p[14]=6.5

p[15]=6.5

p[16]=6.5

x[15]=x_LiBrH2O(T[15],P[15])

x[16]=x_LiBrH2O(T[16],P[16])

q_dotHHE=m_dot[15]*h[15]-m_dot[16]*h[16]

ex[14]=m_dot[14]*((h[14]-h[0])-t[0]*(s[14]-s[0]))

ex[15]=m_dot[15]*((h[15]-h[0])-t[0]*(s[15]-s[0]))

ex[16]=m_dot[16]*((h[16]-h[0])-t[0]*(s[16]-s[0]))

exqHHE=(1-t[0]/(t[14]/4+t[12]/4+t[15]/4+t[16]/4)) *q_dotHHE

exdHHE=ex[12]+exqHHE+ex[15]-ex[14]-ex[16]

"for HTG"

t[21]=480

m_dot[21]=0.088

p[21]=6.5

s[21]=Entropy(H2O,T=T[21],P=P[21])

h[21]=Enthalpy(Water,T=T[21],P=P[21])

m_dot[27]=1

t[27]=503

t[28]=t[27]-150

q_dotgeo=m_dot[27]*cp[27]*(t[27]-t[28])

cp[27]=Cp(Water,T=T[27],P=P[27])

p[27]=200

ex[21]=m_dot[21]*((h[21]-h[0])-t[0]*(s[21]-s[0]))

exqHTG=(1-t[0]/(t[15]/3+t[14]/3+t[21]/3)) *q_dotgeo

exdHTG=ex[14]+exqHTG-ex[15]-ex[21]

"for HTC"

t[22]=144.7+273

m_dot[22]=0.088

h[22]=enthalpy(Water,T=T[22],P=P[22])

p[22]=6.5

s[22]=Entropy(H2O,T=T[22],P=P[22])

q_dotHTC=-m_dot[22]*h[22]+m_dot[21]*h[21]

ex[22]=m_dot[22]*((h[22]-h[0])-t[0]*(s[22]-s[0]))

exqHTC=(1-t[0]/(t[21]/2+t[22]/2)) *q_dotHTC

exdHTC=ex[21]+exqHTC-ex[22]

"for MTC"

t[23]=390

t[25]=340

m_dot[23]=0.088

m_dot[25]=0.1359

h[23]=Enthalpy(Water,T=T[23],P=P[23])

h[25]=Enthalpy(Water,T=T[25],P=P[25])

p[23]=4.5

p[25]=4.5

s[23]=Entropy(Water,T=T[23],P=P[23])

s[25]=Entropy(Water,T=T[25],P=P[25])

q_dotMTC=m_dot[24]*h[24]+m_dot[23]*h[23]-m_dot[25]*h[25]

ex[23]=m_dot[23]*((h[23]-h[0])-t[0]*(s[23]-s[0]))

ex[25]=m_dot[25]*((h[25]-h[0])-t[0]*(s[25]-s[0]))

exqMTC=(1-t[0]/(t[24]/3+t[23]/3+t[25]/3)) *q_dotMTC

exdMTC=ex[23]+ex[24]-ex[25]+exqMTC

"for cond"

t[8]=300

t[26]=330

m_dot[8]=0.1649

m_dot[26]=0.1359

p[26]=1.8

p[8]=1.8

h[8]=Enthalpy(Water,T=T[8],P=P[8])

h[26]=Enthalpy(Water,T=T[26],P=P[26])

s[8]=Entropy(Water,T=T[8],P=P[8])

s[26]=Entropy(Water,T=T[26],P=P[26])

q_dotCOND=m_dot[26]*h[26]+m_dot[7]*h[7]-m_dot[8]*h[8]

ex[8]=m_dot[8]*((h[8]-h[0])-t[0]*(s[8]-s[0]))

ex[26]=m_dot[26]*((h[26]-h[0])-t[0]*(s[26]-s[0]))

exqCOND=(1-t[0]/(t[8]/3+t[26]/3+t[7]/3))*q_dotCOND

exdCOND=ex[7]+ex[26]-ex[8]+exqCOND

"for eva."

t[9]=279

t[10]=280

m_dot[9]=0.1649

m_dot[10]=0.1649

h[9]=Enthalpy(Water,T=T[9],P=P[9])

p[9]=0.93

p[10]=0.93

h[10]=Enthalpy(Water,T=T[10],P=P[10])

s[9]=Entropy(Water,T=T[9],P=P[9])

s[10]=Entropy(Water,T=T[10],P=P[10])

q_dotEVAP=(m_dot[10]*h[10]-m_dot[9]*h[9])

ex[9]=m_dot[9]*((h[9]-h[0])-t[0]*(s[9]-s[0]))

ex[10]=m_dot[10]*((h[10]-h[0])-t[0]*(s[10]-s[0]))

exqEVAP=-((1-t[0]/(t[9]/2+t[10]/2)) *q_dotEVAP)

exdEVAP=ex[9]-ex[10]+exqEVAP

"energy for absor."

m_dot[1]=1

t[1]=303

x[1]=x_LiBrH2O(T[1],P[1])

h[1]=h_LiBrH2O(T[1],x[1])

p[1]=1.5

t[6]=322

h[6]=h_LiBrH2O(T[6],x[6])

p[6]=0.9

m_dot[6]=0.8351

q_dotABS=m_dot[1]*h[1]+m_dot[10]*h[10]+m_dot[6]*h[6]

s[1]=s_LiBrH2O(T[1],x[1])

s[10]=s_LiBrH2O(T[10],x[10])

x[6]=x_LiBrH2O(T[6],P[6])

s[6]=s_LiBrH2O(T[6],x[6])

ex[1]=m_dot[1]*((h[1]-h[0])-t[0]*(s[1]-s[0]))

ex[6]=m_dot[6]*((h[6]-h[0])-t[0]*(s[6]-s[0]))

exqABS=(1-t[0]/(t[1]/3+t[6]/3+t[10]/3))* q_dotABS

exdABS=ex[10]+ex[6]-ex[1]-exqABS

"for pump4"

v[27]=Volume(Water,T=T[27],P=P[27])

p[28]=200

h[27]=Enthalpy(Water,T=T[27],P=P[27])

s[27]=Entropy(Water,T=T[27],P=P[27])

ex[27]=m_dot[27]*((h[27]-h[0])-t[0]*(s[27]-s[0]))

w_dotpump4=(m_dot[27]*(v[28]*(p[30]-p[28])))/0.85

v[28]=Volume(Water,T=T[28],P=P[28])

s[28]=Entropy(Water,T=T[28],P=P[28])

h[28]=Enthalpy(Water,T=T[28],P=P[28])

ex[28]=m_dot[27]*((h[28]-h[0])-t[0]*(s[28]-s[0]))

t[29]=t[28]

p[29]=p[30]

s[29]=Entropy(Water,T=T[29],P=P[29])

h[29]=Enthalpy(Water,T=T[29],P=P[29])

ex[29]=m_dot[27]*((h[29]-h[0])-t[0]*(s[29]-s[0]))

"organic rankin cycle"

"for rankin cycle"

ex[31]=m_dot[31]*((h[31]-h[0])-t[0]*(s[31]-s[0]))

m_dot[31]=m_dot[27]

p[30]=250

t[30]=40+t[28]

s[30]=Entropy(Water,T=T[30],P=P[30])

h[30]=Enthalpy(Water,T=T[30],P=P[30])

cp[30]=Cp(Water,T=T[30],P=P[30])

ex[30]=m_dot[27]*((h[30]-h[0])-t[0]*(s[30]-s[0]))

m_dot[30]=1

t[31]=t[30]-65

q_dotboiler+m_dot[34]*h[34]=m_dot[35]*h[35]

q_dotboiler=(h[30]-h[31])*18.22

m_dot[34]=4

```
m_dot[35]=m_dot[34]

p[31]=p[30]

s[31]=Entropy(Water,T=T[31],P=P[31])

h[31]=Enthalpy(Water,T=T[31],P=P[31])

p[32]=300

m_dot[32]=m_dot[27]

t[32]=t[31]

h[32]=Enthalpy(Water,T=T[32],P=P[32])

ex[32]=m_dot[32]*((h[32]-h[0])-t[0]*(s[32]-s[0]))

s[32]=Entropy(Water,T=T[32],P=P[32])

t[33]=20+273.15

p[33]=900

h[33]=Enthalpy(Ammonia,T=T[33],P=P[33])

s[33]=Entropy(Ammonia,T=T[33],P=P[33])

ex[33]=m_dot[33]*((h[33]-h[0])-t[0]*(s[33]-s[0]))

p[34]=3800

T[34]=20+273.15

s[34]=Entropy(Ammonia,T=T[34],P=P[34])

h[34]=Enthalpy(Ammonia,T=T[34],P=P[34])

"h[35]=Enthalpy(Ammonia,T=T[35],P=P[35])"

p[35]=p[34]

T[35]=90+273

s[35]=Entropy(Ammonia,T=T[35],P=P[35])

x[36]=0.1

s[36]=Entropy(Ammonia,T=T[36],P=P[36])
```

p[36]=p[33]

T[36]=30+273

h[36]=Enthalpy(Ammonia,T=T[36],s=s[36])

"x[36]=0.

h[36]=Enthalpy(Water,T=T[36],x=x[36])"

v[35]=Volume(Water,T=T[35],P=P[35])

w_dotturbine=(m_dot[33]*(h[35]-h[36])/0.85)

q_dotoutcond=m_dot[36]*(h[36]-h[33])

m_dot[36]=m_dot[33]

exqcondrankin=((1-t[0]/(t[36]/4+t[33]/4+t[38]/4+t[39]/4))*q_dotoutcond)

exdcondrankin=ex[36]+ex[38]-exqcondrankin-ex[39]

ex[34]=m_dot[33]*((h[34]-h[0])-t[0]*(s[34]-s[0]))

ex[35]=m_dot[33]*((h[35]-h[0])-t[0]*(s[35]-s[0]))

ex[36]=m_dot[33]*((h[36]-h[0])-t[0]*(s[36]-s[0]))

exdturbine=ex[35]-ex[36]-w_dotturbine

exqboil=((1-t[0]/(t[34]/4+t[35]/4+t[30]/4+t[31]/4))* q_dotboiler)

exdbolier=-ex[35]+ex[34]+exqboil

v[33]=Volume(Ammonia,T=T[33],P=P[33])

m_dot[33]=m_dot[35]

w_dotpump6=m_dot[33]*(v[33]*(p[34]-p[33]))/0.85

w_dotpump5=(m_dot[31]*(v[31]*(p[32]-p[31])))/0.85

v[31]=Volume(Water,T=T[31],P=P[31])

p[37]=101

t[37]=288

v[37]=Volume(Water,T=T[37],P=P[37])

h[37]=Enthalpy(Water,T=T[37],P=P[37])

s[37]=Entropy(Water,T=T[37],P=P[37])

ex[37]=m_dot[37]*((h[37]-h[0])-t[0]*(s[37]-s[0]))

p[38]=300

t[38]=288

w_dotpump7=(m_dot[37]*(v[37]*(p[38]-p[37])))/0.85

m_dot[37]=50

m_dot[38]=50

m_dot[38]*h[38]+q_dotoutCOND=m_dot[38]*h[39]

h[38]=Enthalpy(Water,T=T[38],P=P[38])

s[38]=Entropy(Water,T=T[38],P=P[38])

ex[38]=m_dot[38]*((h[38]-h[0])-t[0]*(s[38]-s[0]))

p[39]=p[38]

T[39]=Temperature(Water,P=P[39],h=h[39])

s[39]=Entropy(Water,T=T[39],P=P[39])

ex[39]=m_dot[39]*((h[39]-h[0])-t[0]*(s[39]-s[0]))

m_dot[39]=50

ex[33]+w_dotpump6=ex[34]+exdpump6

ex[31]+w_dotpump5-ex[32]=exdpump5

ex[28]+w_dotpump4-ex[29]=exdpump4

Q_dotHW=m_dot[27]*cp[32]*(t[32]-t[0])

cp[32]=Cp(Water,T=T[32],P=P[32])

ex[11]=200

ex[13]=200

ex[44]=200

ex[45]=200

N=46

EX_total=SUM(ex[i], i=1,N)

Exd_total=exdpump4+exdpump5+exdpump6+exdH2+exddihumidification+exdbolie

r+exdturbine+exdcondrankin+exdABS+exdEVAP+exdCOND+exdMTC+exdHTC+

exdHTG+exdHHE+exdMTG+exdMHE+exdLTG+exdLHE

F_ei=Exd_total/EX_total

C_ei=1/(ep.totalex)

teta_ei=F_ei*C_ei

teta_eii=1/teta_ei

F_es=EX_total/(EX_total+Exd_total)

teta_est=F_es*teta_eii